SUPELEC

HEAT SINK ANALYTICAL MODELING

Master thesis

Joaquim Guitart Corominas

March 2011

Tutor : Amir ARZANDÉ

Département d'Electrotechnique et de Systèmes d'Energie

École Supérieure d'Électricité

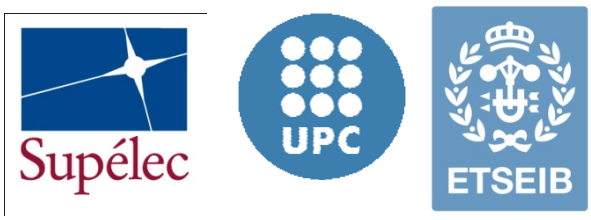

1 Introduction

Electronics has leaded most technological advances of the past 60 years.

There are technologies with domains particularly developed for electronics such as material science, electromagnetism, system dynamics and also heat transfer.

The relation to heat transfer is because the heat generation of electronics devices. Commonly, these devices need additional cooling in order to avoid extreme temperatures inside it. Heat sinks allow this supplementary cooling, so they are omnipresent in electronic assemblies.

Heat sink can work by forced convection, natural convection or liquid cooling. Normally in electronic assemblies they are made of materials with good thermal conduction such as aluminum or copper. The heat transfer in sinks is especially by convection, but also by radiation. Radiation heat transfer can represent up to 30% of heat rate in natural convection heat sinks.

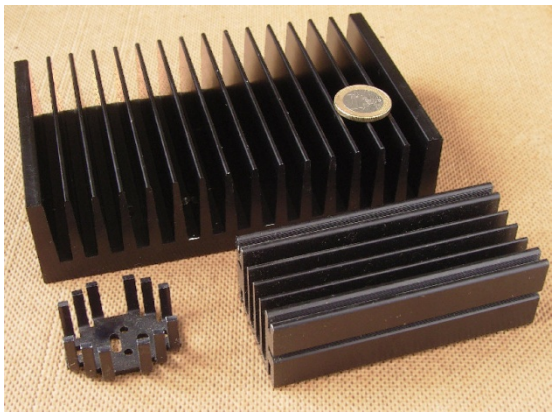

The manufacturing process is usually by extrusion, but also by cast, bonded, folded, skived and stamped processes.

There are a lot of geometries available and they are generally adapted to each specific requirement. However, a very common heat sink profile is the rectangular parallel fin one. This profile forms U-channels, where the convection phenomenon is able to be modeled by empirical correlations.

The radiation process is almost a geometric problem, so its analysis will be a minor order study.

The modeling of rectangular parallel fin heat sinks allows an analytical study. This study can lead to determining the parameters of a heat sink for a specific application, mainly for electronics industry.

The heat transfer processes that occur in a heat sink are studied in this work. There is also proposed an algorithm for rectangular parallel fin heat sinks and the computation study of its results. These computation results are compared to a finite element program solution in order to know the error of the proposed model. Finally, is suggested an optimization application for this algorithm.

2 Heat generation in electronic devices

The power electronic devices are made with PN structures that have heat losses when current circulates across it. The overheating can destroy the PN structure, in which junctions are the most sensible part.

There are some phenomenons that produce heat losses in PN structures.

- Conduction losses. When a PN junction allows the current circulations, there is a potential drop between the PN terminals that produce heat. The heat generated in conduction status can be expressed as:

$$q_h = R_{ON} \cdot I_{ON}^2 \tag{1}$$

- Blocking losses. A residual current remains when the device is in blocking position.
- Switching losses. The current and voltage switches are not instantaneous. When a PN diode is in a conduction state and is going to be a blocking state a transient negative current is present as the blocking voltage is being applied: it is called recovery phenomenon. Therefore, the switching frequency is an important factor to take into account when heat losses are analyzed.
- Driving losses.

2.1 IGBT

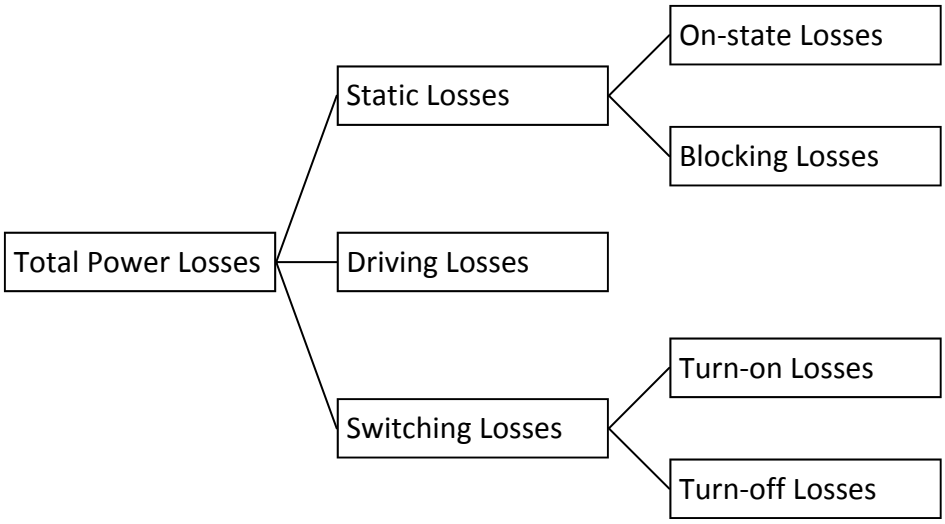

Fig. 1 Power losses in electronics devices.

Because they are only contributing to a minor share of the total power dissipation, forward blocking losses and driver losses may usually be neglected.

On-state power dissipations ($P_{fw/T}$) are dependent on:

- Load current (over output characteristic $v_{CEsat} = f(i_C, v_{GE})$)
- Junction temperature $T_{j/T}$ (K)
- Duty cycles D_T

For given driver parameters, the turn-on and turn-off power dissipations ($P_{on/T}$, $P_{off/T}$) are dependent on:

- Load current v_d (V)
- DC-link voltage i_{LL}(A)
- Junction temperature $T_{j/T}$ (K)
- Switching frequency f_s (1/s)

The total losses $P_{tot/T}$ for an IGBT can be expressed as:

$$P_{tot/T} = P_{fw/T} + P_{on/T} + P_{off/T} \quad (2)$$

Where:

Power generated per switch-on (W)

$$P_{on/T} = f_s \cdot E_{on/T}(v_d, i_{LL}, T_{j/T})$$

Power generated per switch-off (W)

$$P_{off/T} = f_s \cdot E_{off/T}(v_d, i_{LL}, T_{j/T})$$

On-state power dissipation (W)

$$P_{fw/T} = i_{Lavg} v_{CEsat}(i_{Lavg}, T_{j/T}) D_T$$

Where $E_{on/T}(v_d, i_{LL}, T_{j/T})$is the heat generated per switch-on (J), $E_{off/T}(v_d, i_{LL}, T_{j/T})$ is the heat generated per switching-off (J), i_{Lavg} is the average load current (A), D_T is the transistor duty cycle, $v_{CEsat}(i_{Lavg}, T_{j/T})$ is the Collector-emitter saturation voltage (V)

2.2 DIODE

Because they are only contributing to a minor share of the total power dissipation, reverse blocking power dissipations may usually be neglected. Schottky diodes might be an exception due to their high-temperature blocking currents.

Turn-on power dissipations are caused by the forward recovery process. As for fast diodes, this share of the losses may mostly be neglected as well.

On-state power dissipations ($P_{fw/D}$) are dependent on:

- Load current (over forward characteristic $v_F = f(i_F)$)
- Junction temperature T_{jD}
- Duty cycles D_D

For a given driver setup IGBT commutating with a freewheeling diode, turn-off power losses (P_{off}/D) depend on:

- Load current

- DC-link voltage
- Junction temperature $T_{j/D}$ (K)
- Switching frequency f_s (1/s)

$$P_{tot/D} = P_{fw/D} + P_{off/D} \quad (3)$$

Where:

Power generated per switch-off (W) $$P_{off/D} = f_s \cdot E_{off/D}(v_d, i_{LL}, T_{j/D})$$

Forward power dissipation (W) $$P_{fw/T} = i_{Lavg} v_F(i_{Lavg}, T_{j/D}) D_D$$

Where $E_{off/D}(v_d, i_{LL}, T_{j/D})$ is the heat generated per switching-off (J), i_{Lavg} is the average load current (A), D_D is the transistor duty cycle.

3 Introduction to heat transfer

The heat sinks are elements that prevent the destruction of electronic equipment because of its overheating. The most critical part in an electronic device is the semiconductor junction. The junction temperature can't exceed a temperature given by the manufacturer.

The heat sinks have different shapes depending on the nature of the coolant fluid (natural air convection cooling, forced air convection cooling, liquid cooling...), the manufacturing process, the electronic module packaging…

To facilitate the understanding of heat transfer laws for electric engineers, it can be useful to explain this as an analogy between electrical and thermal resistances.

The Ohm's law describes the relation between the current I, the potential difference ΔV and the resistance R between two points as:

$$I = \frac{\Delta V}{R} \tag{4}$$

In the thermal analogy, the potential difference ΔV (V) is associated to temperature difference between two points ΔT (ºC), the electrical resistance R (Ω) is associated to a thermal resistance R (C/W), and the current (A) is associated to a heat flux ratio Q (W).

$$Q = \frac{\Delta T}{R} \tag{5}$$

The number of resistances of a model depends on the desired precision. A high precision model requires a large number of resistances. However, a high number of resistances in a model can reduce significantly the computation speed. Consequently, there is a compromise between the computation speed and the precision of the results.

Generally, the heat ratio Q is determined by the operating conditions of the semiconductor. The temperature increase ΔT, is also determined by the maximum junction temperature and the highest ambient temperature in hypothetical extreme ambient conditions. Therefore, using the equation (5), the highest thermal resistance of an assembly is fixed.

4 The resistances in a heat sink model

The goal of the analysis is to determine the heat sink geometry and a device setup which allow enough heat dissipation for a given devices and working conditions.

The heat sinks can be meshed by many 3D thermal resistances which can involve a complex modeling. For simple analytical analysis, there is no more than one heat source involved; it is useful to use the one dimensional method of equivalent resistances.

In this lineal system, the global resistance R can be divided into three thermal resistances R_{sa}, R_{cs} and R_{jc} (fig 2). The addition of these three resistances is the global resistance R, given in equation (6).

$$R = R_{sa} + R_{cs} + R_{jc} \quad (6)$$

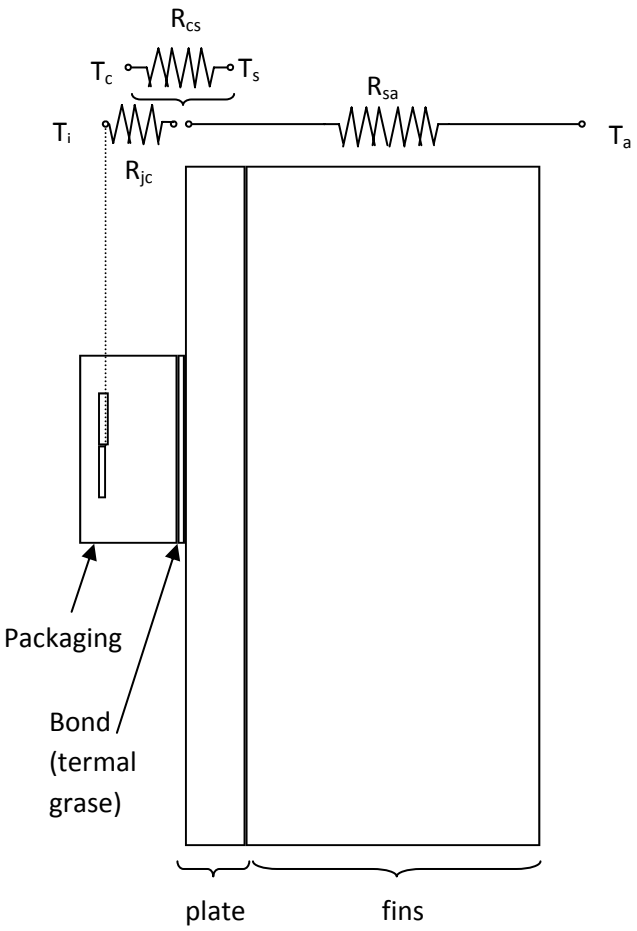

Fig. 2 Resistances in a heat sink

R_{jc} is the resistance between the surface of the device and the junction of the semiconductor. It is usually given by the device manufacturer.

R_{cs} is the resistance between the device and the heat sink. It depends on factors such as the assembly method, the surface roughness and the thermal grease type. It takes frequently low range values, and it can be neglected in most models.

R_{sa} is the resistance between the surface of the plate next to the device, and the ambient. It is the resistance of the heat sink for itself and it involves radiation, convection and conduction heat transfer. The radiation and conduction can be calculated precisely using analytical approaches. However, the convection heat transfer requires semi empirical correlations which can vary notably depending on the author and the flux conditions.

Therefore, the calculation of R_{sa} requires an extended analysis.

4.1 Sink ambient resistance R_{sa}

The analysis leads to a division of the heat sink resistance R_{sa} into three sub-resistances.

$$R_{sa} = R_{bf} + R_{sp} + R_{fa} \quad (7)$$

R_{bf} is the resistance due to the limited conduction of a flat plate when a uniform flux flows perpendicularly to its surface.

R_{sp} is a resistance due to the flux spreading penalization. When a flux flows through a plate from a heat source area S1 to a dissipation area S2 and S2>S1, then the flux flow is not completely perpendicularly and spreading resistance appears.

R_{fa} is the resistance between the plate surface that supports the fins, and the ambient. The heat is driven away due to convection and radiation heat transfer. The fins have also a conductive resistance as a result of its finite thermal conductivity.

All these resistances will be explained accurately in the next sections.

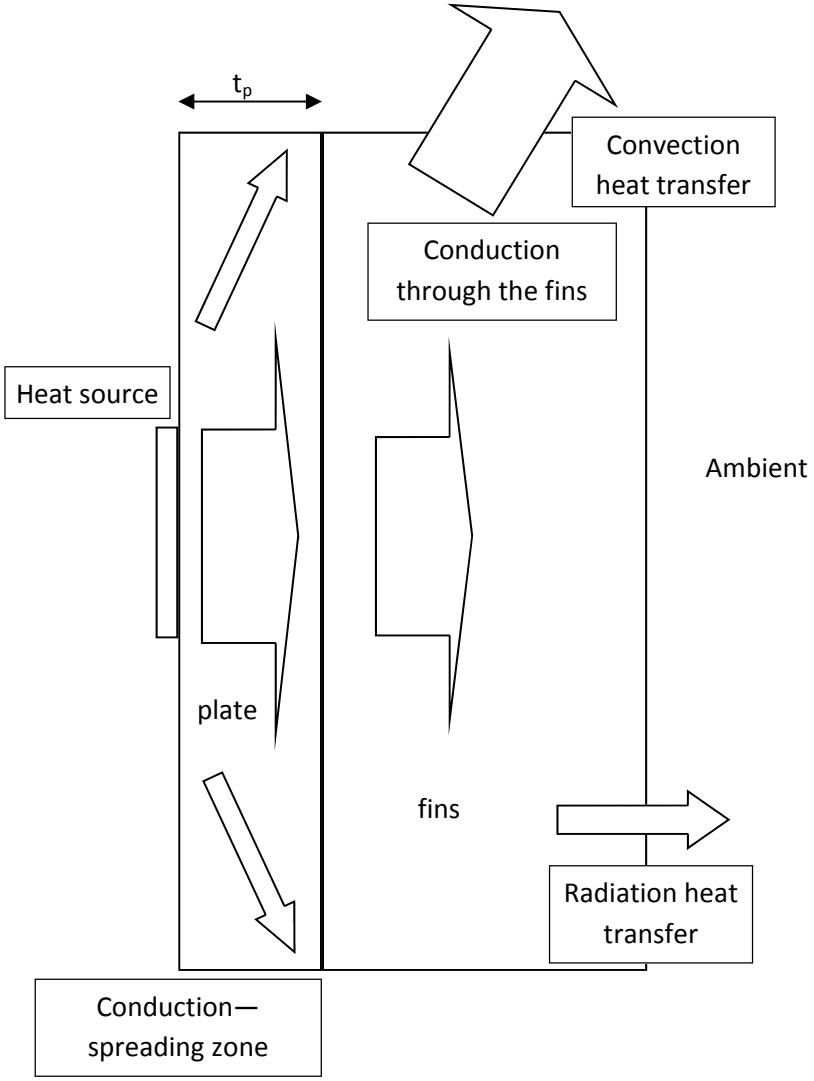

Fig. 3 Heat sink common fluxes

4.2 R_{bf} Plate conduction resistance

It is directly calculated using the equation 5

$$R_{bf} = \frac{t_p}{k \cdot A} \tag{8}$$

Where k is the plate conductivity (W/K·m), A is the heat transfer area (m^2) and t_p is the plate thickness.

As an introduction to conduction heat transfer, the demonstration of equation (8) is developed below.

4.2.1 Conduction heat transfer

The following equation (9) is deduced from the energy balance in a control volume in Cartesian coordinates.

$$\frac{\partial}{\partial x}\left(k\frac{\partial T}{\partial x}\right)+\frac{\partial}{\partial y}\left(k\frac{\partial T}{\partial y}\right)+\frac{\partial}{\partial z}\left(k\frac{\partial T}{\partial z}\right)+\dot{q}=\rho C_p\frac{\partial T}{\partial t} \quad (9)$$

Where k is the plate conductivity (W/K·m), $\dot{q}$ in the internal heat generation (W/m^3), ρ in the material density (Kg/m^3), C_p is the heat capacity of the material (J/Kg·K), T is the temperature and t is the time.

In steady state conditions, $\frac{\partial T}{\partial t}=0$, in uniform flux flow through x axis $\frac{\partial}{\partial y}\left(k\frac{\partial T}{\partial y}\right)+\frac{\partial}{\partial z}\left(k\frac{\partial T}{\partial z}\right)=0$ and in materials without heat generation $\dot{q}$=0, the equation (9) is reduced to equation (10):

$$\frac{d}{dx}\left(k\frac{dT}{dx}\right)=0 \quad (10)$$

Integrating the equation (10) and applying the boundary conditions $T(0)=T_0$ and $T(L)=T_L$ the temperature distribution through the wall can be expressed as:

$$T(x)=\left(T_{s,2}-T_{s,1}\right)\frac{x}{t_p}+T_{s,1} \quad (11)$$

The Fourier Law for on dimensional flux can be expressed as:

$$q_x=-k\cdot A\cdot\frac{dT}{dx} \quad (12)$$

Where q_x is the heat flux (W) in x direction, k is the plate conductivity (W/K·m) and A is the heat transfer area (m^2).

The derivate of equation (11) is calculated as:

$$\frac{dT}{dx}=\frac{\left(T_{s,2}-T_{s,1}\right)}{t_p} \quad (13)$$

Substituting the expression (13) in Fourier's equation (12):

$$q_x=-\frac{k\cdot A}{t_p}\left(T_{s,2}-T_{s,1}\right)=\frac{k\cdot A}{t_p}\left(T_{s,1}-T_{s,2}\right) \quad (14)$$

Finally, the thermal resistance R_{bf} is deduced as:

$$\boldsymbol{R_{bf}} = \frac{\Delta T}{q_x} = \frac{(T_{s,1} - T_{s,2})}{\frac{k \cdot A}{t_p}(T_{s,1} - T_{s,2})} = \frac{\boldsymbol{t_p}}{\boldsymbol{k \cdot A}} \quad (15)$$

4.3 R_{sp} resistance

The R_{sp} resistance is due to the flux spread through the plate thickness. A plate has two sides. In one side there is the heat source, and in the other side there are the fins that dissipate the heat. The source area is usually smaller than the dissipation area. The flux direction inside the plate becomes not-perpendicular to the surface and it involves a resistance associated.

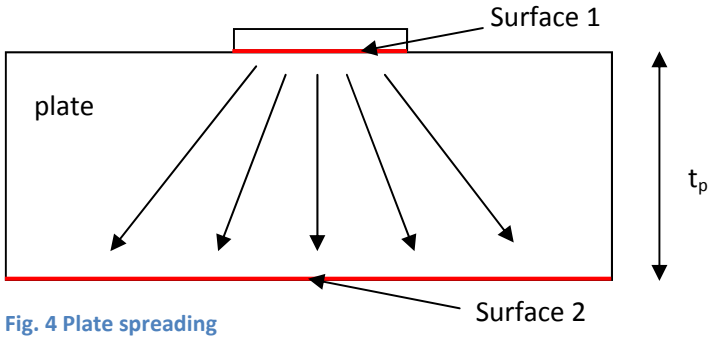

Fig. 4 Plate spreading

The works of Yovanovich and Antonetti lead to the following expression for a heat source centered in heat sink surface:

$$R_{sp} = \frac{1 - 1.410\epsilon + 0.344\epsilon^3 + 0.043\epsilon^5 + 0.034\epsilon^7}{4ka} \quad (16)$$

Where ϵ is the ratio between the heat transfer surface 1 and the heat transfer surface 2, k is the plate conductivity (W/K·m) and a is the square root of surface 1: $a = \sqrt{surface1}$.

4.4 R_{fa} resistance

The resistance between the plate surface that supports the fins and the environment is the R_{fa} resistance. This resistance includes conduction, convection and radiation heat transfer. The Newton's law of cooling (17) is a linear expression that can be used to find the resistance R_{fa} in (18).

$$q = h \cdot A \cdot (T_s - T_{amb}) \quad (17)$$

Where q is the heat transfer rate (W), h is the convection coefficient (W/K·m^2), A is the heat transfer surface (m^2), T_s is the surface temperature (K) and T_{amb} is the ambient temperature (K).

$$R_{fa} = \frac{q}{(T_s - T_{amb})} = \frac{1}{h \cdot A} \quad (18)$$

However, this expression does not include the conduction resistance through the fins and the radiation heat transfer. That will lead to modify the expression (17) into the expression (19) in order to include all heat transfer phenomenon.

$$q = (h_c + h_r) \cdot (A_p + \eta \cdot A_f) \cdot (T_s - T_{amb}) \quad (19)$$

Where q is the heat transfer rate (W), h_c is the convection coefficient (W/K·m^2), h_r is the radiation equivalent coefficient (W/K·m^2), A_p is the primary area (m^2), A_f is the extended area (m^2), η is the fin efficiency, T_s is the plate surface temperature (K) and the T_{amb} is the ambient temperature (K).

All these variables and coefficients will be explained in the next sections.

4.4.1 Fin conduction factor: $(A_p + \eta \cdot A_f)$

Fins have a finite conductivity. It means that the temperature can vary along its surface. But in equation (19) the T_s is included as a fixed value, it is not a function like $T_s(x)$. For this, the fin efficiency is included to penalize the temperature variation along the fin surface without affecting the linearity of equation (19). This efficiency will modify the affected surface A_f of the fin, but the primary plate surface A_p will retain the expected temperature T_s and it will be not affected by the efficiency (fig 5).

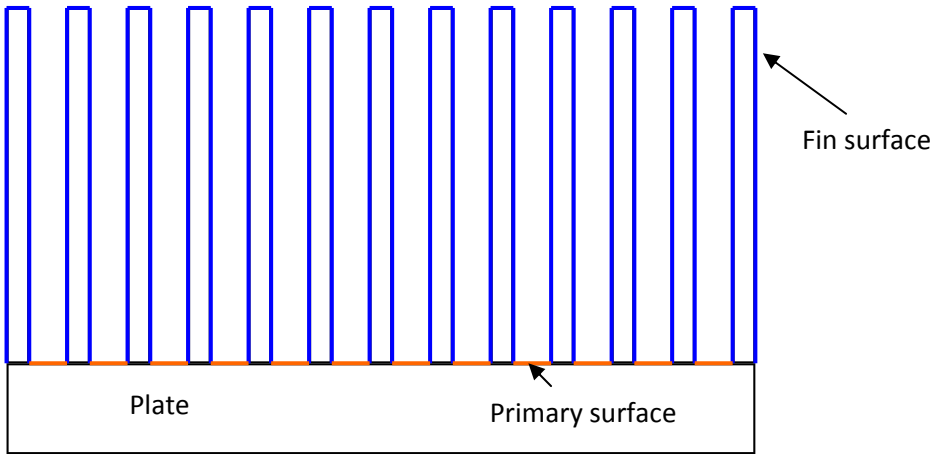

Fig. 5 Surfaces in a parallel plate heat sink

The efficiency depends on the fin geometry. In industry there are a lot of fin profiles available (fig 7), from pin fins to hyperbolic profile longitudinal fins. A rectangular profile fits accurately the most longitudinal profiles (fig 6), so it will be used in the proposed analytical model.

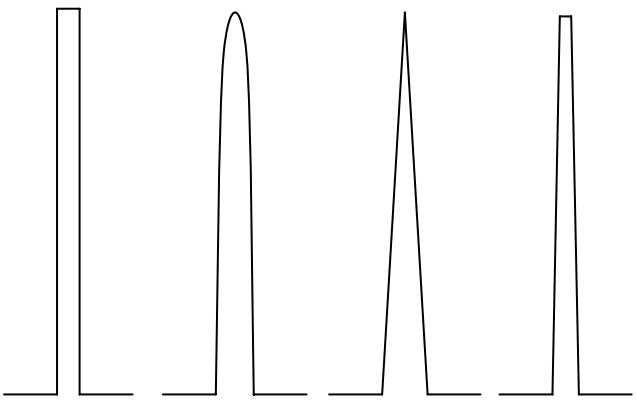

Fig. 7 Rectangular profile, hyperbolic profile, triangular profile, trapezoidal profile

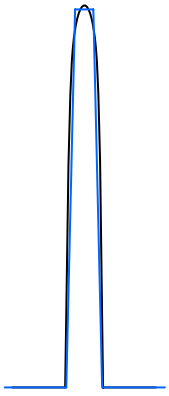

Fig. 6 Superposition of a trapezoidal and a hyperbolic profile fin.

4.4.1.1 *Efficiency analysis η*

From Fourier's equations (12) and from energy balance equations (9), is deduced:

$$\frac{d^2T}{dx^2} + \left(\frac{1}{A_c}\frac{dA_c}{dx}\right)\frac{dT}{dx} - \left(\frac{1}{A_c}\frac{h}{k}\frac{dA_s}{dx}\right)(T - T_\infty) = 0 \qquad (20)$$

Where h is de convection coefficient (W/Km^2), k is the thermal conductivity of the fin (W/Km) and the remaining parameters are shown in Fig. 7.

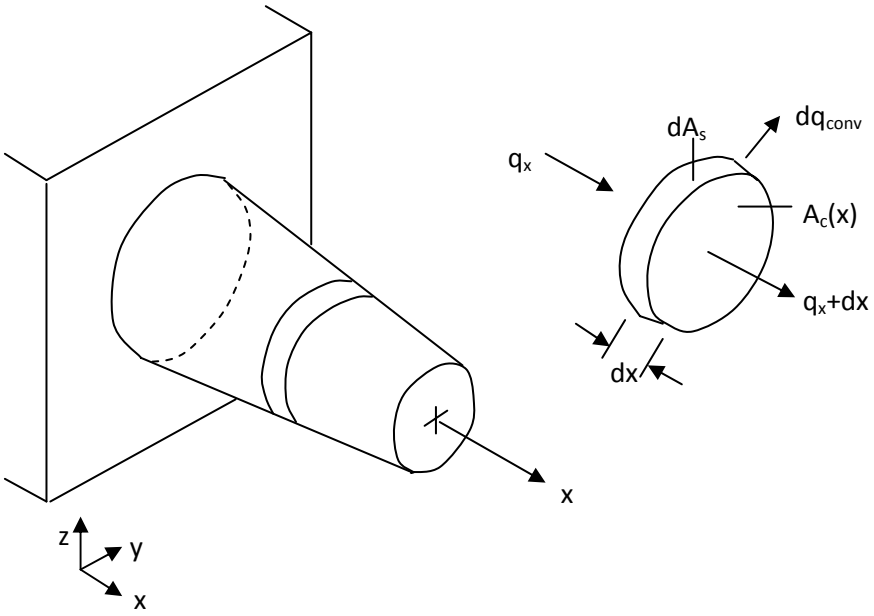

Fig. 8 Fin profile

4.4.1.2 *Rectangular longitudinal fins demonstration*

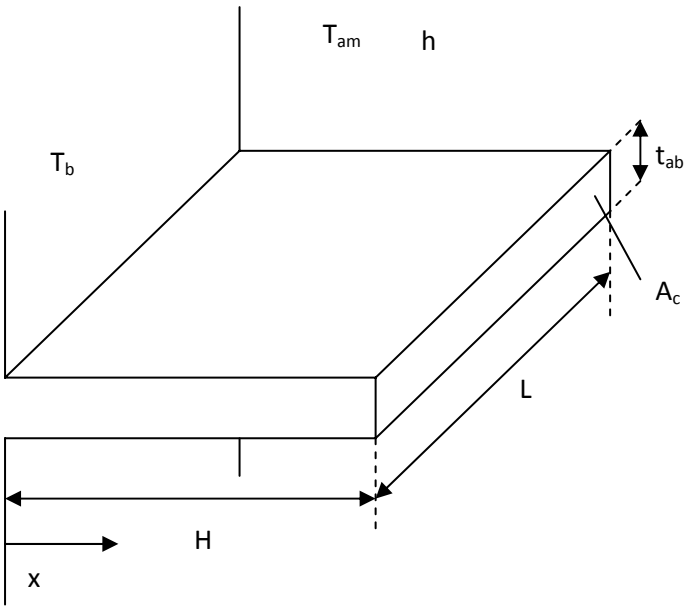

Fig. 9 Rectangular longitudinal profile

In this case, the section A_c is constant. If P is assumed as the section perimeter:

$$\frac{d^2T}{dx^2} - \frac{h \cdot P}{k \cdot A_c}(T - T_\infty) = 0 \qquad (21)$$

Replacing

$$\theta(x) = T(x) - T_\infty \qquad (22)$$

$$m = \sqrt{\frac{h \cdot P}{k \cdot A_c}}$$

A second order differential equation is obtained:

$$\frac{d^2\theta}{dx^2} - m\theta = 0 \tag{23}$$

The restrictions are adiabatic tip (x=H) and fixed base temperature T_b.

$$\left.\frac{d\theta}{dx}\right|_{x=H} = 0 \qquad \theta_b = T_b - T_\infty \tag{24}$$

The solution of equation (23) applying restrictions (24) is:

$$\theta(x) = \frac{\cosh\{m(H-x)\}}{\cosh(mH)}\theta_b \tag{25}$$

Where *H* is the fin high (m).

To know the power dissipated, the heat transfer at the fin base is analyzed.

$$q_b = kA\left.\frac{d\theta}{dx}\right|_{x=0} \tag{26}$$

Substituting $\left.\frac{d\theta}{dx}\right|_{x=0}$ for the derivative of equation (25):

$$q_b = \sqrt{hPkA_c}\cdot\theta_b\tanh(mH) \tag{27}$$

The efficiency is the ratio between the maximum heat rate that a perfect fin can dissipate and the heat rate that dissipate a real fin. The maximum power that can dissipate a perfect fin is deduced from the Newton's law of cooling (17), expressed as:

$$q_{max} = h\cdot A\ \cdot(T_b - T_{amb}) = hA_f\theta_b \tag{28}$$

Where A_f the fin area and T_b is the fin base temperature.

From equation (27) and equation (28) is deduced the fin efficiency assuming t_{ab}<<*L*.

$$\eta = \frac{q_b}{q_{max}} = \frac{q_b}{hA_f\theta_b} = \frac{\sqrt{hPkA_c}\cdot\theta_b\tanh(mH)}{hPH\theta_b} = \frac{\tanh(mH)}{mH} \tag{29}$$

This equation is also valid for a convective fin tip, $\left.\frac{d\theta}{dx}\right|_{x=H} \neq 0$ substituting the parameter *H* in (29) for H_c.

$$H_c = H + \frac{t_{ab}}{2}$$

4.4.1.3 Trapezoidal longitudinal fins equations

As mentioned before, the trapezoidal fin profile will be used in the modeling of heat sinks due to its fitness to most fin profiles.

The equations that determine the efficiency of the fins are:

$$\eta = \frac{\mu_b}{2K^2 H_c} \cdot \frac{K_1(\mu_a)I_1(\mu_b) - I_1(\mu_b)K_1(\mu_b)}{I_0(\mu_b)K_1(\mu_a) + I_1(\mu_a)K_0(\mu_b)} \tag{30}$$

Where:

$$H_c = H + t_{af}/2 \tag{31}$$

$$\kappa = \text{atan}\left(\frac{t_{ab} - t_{ab}}{2H_c}\right) \tag{32}$$

$$K = \sqrt{\frac{\bar{h}}{k \cdot \sin(\kappa)}} \tag{33}$$

$$\mu_a = 2K\left[\frac{t_{af}(1 - \tan(\kappa))}{2\tan(\kappa)}\right]^{1/2} \tag{34}$$

$$\mu_b = 2K\left[H_c + \frac{t_{af}(1 - \tan(\kappa))}{2\tan(\kappa)}\right]^{1/2} \tag{35}$$

All parameters used are defined in the Fig. 10 bellow:

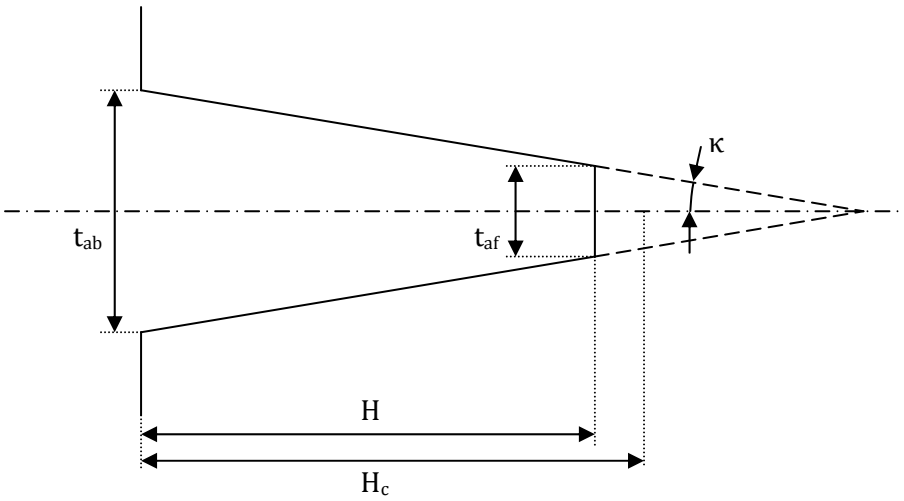

Fig. 10 Trapezoidal longitudinal fin profile

4.4.2 Convection coefficient h_c

The convection is a phenomenon that allows the heat exchange between a solid and a fluid. Even though the Newton's law of cooling (17) is a linear expression, the analysis of the coefficient *h* and the surface temperature T_s can become so complex. The reason is that the convection coefficient depends basically on the temperature, the geometry and the flux regime, but a real surface cannot have a constant temperature.

The chapter 5 explains basic notions of fluid dynamics, which are required to study the convection.

4.4.3 Radiation equivalent coefficient h_r

All bodies emit electromagnetic radiation due its temperature. The heat transferred by radiation depends on the body temperature and the ambient temperature. The heat transfer rate q_r for a body can be expressed as:

$$q_r = A \cdot \varepsilon \cdot \sigma \cdot \left(T_s^4 - T_{amb}^4\right) \tag{36}$$

Where *A* is the body surface (m^2), ε is the surface emissivity (dimensionless), σ is the Stefan - Boltzmann constant (W/m^2K^4), T_s is the surface temperature (K) and T_{amb} is the ambient temperature (K).

So, it is deduced by the equation (36) that the most influent parameter is the temperature difference between the surface and the ambient.

The value of the Stefan–Boltzmann constant is given in SI by:

$$\sigma = 5.6704 \times 10^{-8} \frac{W}{m^2 K^4} \tag{37}$$

The emissivity ε is usually given by the manufacturer, either giving the finish type (degreased, black anodize, clear anodize…) either giving directly the surface emissivity value.

The equation (36) is proposed for surfaces which only emit radiation to the surrounding. However, some shapes forms include surfaces which emit radiation to the surroundings and to other surfaces simultaneously. The equation of these geometries includes a view factor.

The view factor is the proportion of all that radiation which leaves a surface *A* and strikes surface *B*.

4.4.3.1 Radiation in heat sinks

The heat sinks geometry is complicated concerning the radiation analysis. Some surfaces exchange radiation each other and to the ambient simultaneously. Other surfaces exchange radiation only to the ambient. Therefore, the radiation in heat sinks involves more parameters than expressed in equation (36).

The article of Younes Shabany [1], simplifies the radiation in heat sinks. The heat transfer rate q_r (W) can be expressed as:

$$q_r = (n_a - 1)q_{ch,r} + A_d \sigma \varepsilon \left(T_s^4 - T_{amb}^4\right) \tag{38}$$

Where n_a is the number of fins, $q_{ch,r}$ is the heat transfer rate in channel surfaces (W), A_d is the area of all surfaces those radiation does not strike other surfaces (m^2), ε is the body emissivity, σ is the Stefan–Boltzmann constant (W/m^2K^4), T_s is the surface temperature (K) and T_{amb} is the ambient temperature (K).

A_d can be deduced by:

$$A_d = n_a\left(L \cdot t_{af} + 2 \cdot H \cdot \left(\frac{t_{af} + t_{ab}}{2}\right)\right) + 2 \cdot H \cdot L + 2 \cdot t_p(L + w) \tag{39}$$

All parameters of equation (39) are defined in Fig. 11.

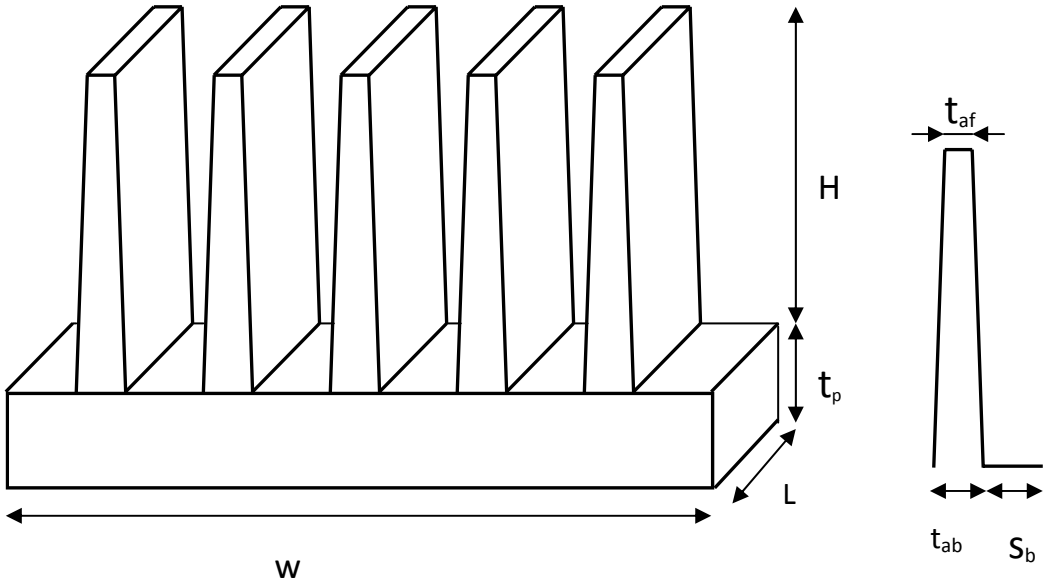

Fig. 11 Heat Sink geometric parameters

The heat transfer rate of a channel can be written as:

$$q_{ch,r} = \frac{\sigma(s_m + 2H)L\left(T_s^4 - T_{amb}^4\right)}{\frac{1-\varepsilon}{\varepsilon} + \frac{1}{F_{s-surr}}} \tag{40}$$

Where $F_{s\text{-}surr}$ is the view factor from the channel surface to the surroundings

Assuming an error, $F_{s\text{-}surr}$ can be written as:

$$F_{s-surr} = 1 - \frac{2\overline{H}\left[\left(1 + \overline{L}^2\right)^{0.5} - 1\right]}{2\overline{H} \cdot \overline{L} + \left(1 + \overline{L}^2\right)^{0.5} - 1} \tag{41}$$

Where:

$$\overline{H} = \frac{H}{s_m} \qquad\qquad \overline{L} = \frac{L}{s_m}$$

And s_m is the average inter fin space.

In order to know the equivalent convection coefficient h_r, is proposed the next equation (42):

$$h_c = \frac{q_r}{(A_p + A_f)(T_s - T_{amb})} \quad (42)$$

Where A_p and A_f are the surfaces (m^2) defined in Fig. 5 and q_r (W) is the heat transfer rate by radiation.

5 Introduction to fluids dynamics

Fluid dynamics analyses the behavior of a fluid when forces are applied to it.

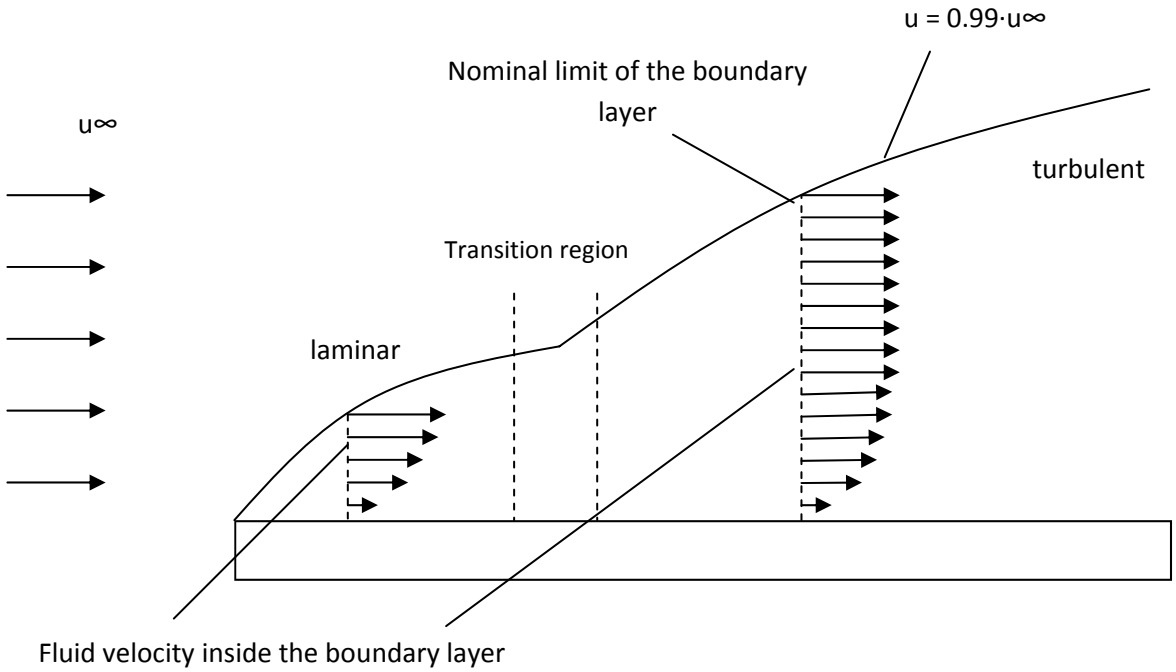

Fig. 12 Velocity regimes through a surface

When a flux flows over a fixed surface, the fluid particles speed the next to the surface is zero. These particles also affect to the contiguous particles, and a speed gradient appears. The nominal limit of the zone affected by the surface is a layer called velocity boundary layer, where the particles have the 99% of the free stream flow velocity.

The movement of the particles next to the surface edge is orderly. This is the laminar flow zone, where the velocities vectors are parallel each other. From a certain point, the particles movements become chaotic. This is the turbulent zone.

Between the laminar and turbulent zone, there is a transition zone. In this region, the first turbulences appear, and after that, the fluid is completely turbulent.

In the laminar zone, the viscous forces are stronger than the movement forces. Contrary, after the transitions zone the movement forces exceed the viscous ones.

The Reynolds number *Re* is a ratio between the movement forces and viscous forces.

$$Re_L = \frac{u_\infty \cdot L}{\nu} \tag{43}$$

Where u_∞ is the mean fluid velocity, *L* is a characteristic linear dimension (m) and v is the kinematic viscosity (m^2/s). The Reynolds number determines the fluids regime for a given surface.

Similarly, the thermal behavior of the fluid has a boundary layer. The nominal limit of the thermal boundary layer is the 99% of the free stream fluid temperature.

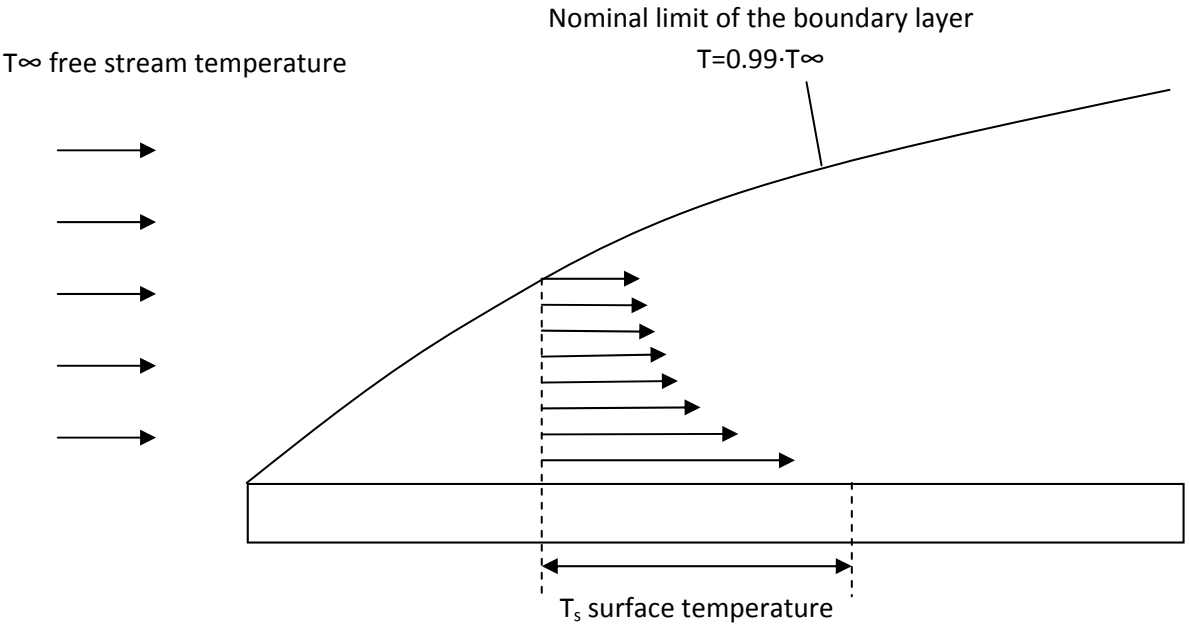

Fig. 13 Flux thermal behavior

The thermal diffusivity α determines the adjustment speed of the fluid temperature to that one of their surroundings. It can be calculated by:

$$\alpha = \frac{k}{\rho C_p} \tag{44}$$

Where k is the fluid thermal conductivity (W/K·m), ρ is the fluid density (Kg/m^3) and C_p is the fluid heat capacity (J/Kg).

The Prandtl number Pr is the ratio of momentum diffusivity to thermal diffusivity. It can be written as:

$$Pr = \frac{\nu}{\alpha} = \frac{C_p \cdot \mu}{k} \tag{45}$$

Where μ is the dynamic viscosity (Kg/m·s). The relation between kinematic and dynamic viscosity can be expressed as:

$$\nu = \frac{\mu}{\rho} \tag{46}$$

The Nusselt number Nu is the ratio of convective to conductive heat transfer. It can be expressed as:

$$Nu = \frac{h \cdot L}{k} \tag{47}$$

Where *L* is a characteristic linear dimension (m).

The Grashof number is the ratio of flotation forces and viscous forces. This number is very significant in natural convection problems. It can be written as:

$$Gr = \frac{g \cdot \beta \cdot (T_s - T_\infty) \cdot L^3}{\nu^2} \tag{48}$$

Where g is the gravity acceleration (m/s^2), β is the thermal expansion coefficient (1/K), T_s is the surface temperature and L is a characteristic linear dimension (m).

The Rayleigh number is the product of Grashof and Nusselt numbers. It determines the type of heat transfer in a fluid. In low range values the heat transfer is basically by conduction. After a critical value, the convection heat transfer type predominates.

$$Ra = Gr \cdot Pr \tag{49}$$

5.1 Developing and fully developed flow

These are concepts that will be taking into account in most convection models.

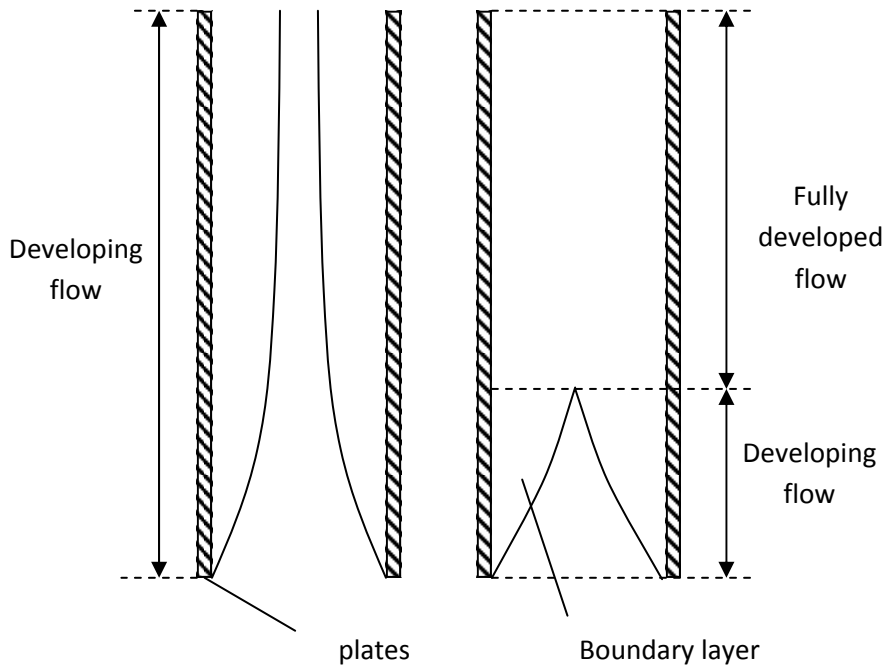

Fig. 14 Boundary layers in developed and fully developed flow

In developing flow between two parallel plates, the boundary layers do not touch each other. Contrary, in the fully developed flow the layers are mixed and the nominal limit of the boundary layer disappears. These two regimes are ruled by different equations, which are usually combined in one expression. In low range Rayleigh numbers, the fully developed flow domains, while in large range Rayleigh numbers, the developing flow domains. The developing flow region length depends on the fluid type, the flow condition and the geometry.

5.2 Convection coefficient in natural convection

The natural convection occurs when a surface heats fluid particles. These particles become more or less dense than the environment ones. Under the gravity action, the less dense fluid particles rise, and the more dense particles fall. Therefore, a relative movement between the heat and cold flow is inducted.

5.2.1 Parallel plates

Elenbaas [2] modeled semi empirically the convection coefficient between parallel plates and ambient. The convection coefficient can be expressed as:

$$h = \frac{\overline{Nu}_{Sm} \cdot k_f}{s_m} \tag{50}$$

Where k_f is the fluid conductivity, $\overline{Nu}_{Sm}$ is the average Nusselt number and s_m is the inter fin space.

Specifically in the case of isothermal parallel plates, the Nusselt number is defined as:

$$\overline{Nu}_{Sm} = \left[\frac{576}{(Ra_{Sm} \cdot s_m/L)^2} + \frac{2.87}{(Ra_{Sm} \cdot s_m/L)^{1/2}}\right]^{-1/2} \tag{51}$$

Where Ra_{Sm} is the Rayleigh number with s_m as a characteristic linear dimension and L is the fin length.

Then, the convection coefficient h is deducted by the equation (40) with s_m as a characteristic linear dimension.

The equation (51) is a composite solution between the fully developed equation and the isolated plate ones, where the developing flow domains.

5.2.2 Natural convection in U channel

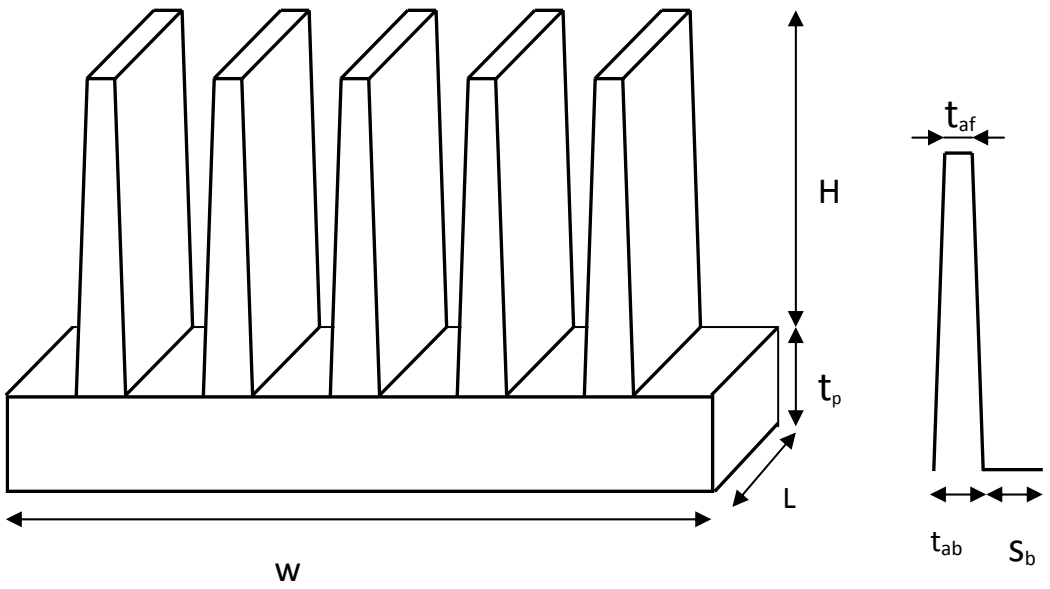

Fig. 15 Heat sink parameters

In the heat sinks, the fins are located on a plate (Fig. 15) and there is also the influence of the plate in the flow. Therefore, a convection model for convectional U channel heat sinks is needed.

5.2.2.1 *Work of Yovanovich*

The article [3] of Yovanovich (1995), proposes a model for rectangular heat sinks, in a relative large Rayleigh number values. The characteristic length is taken as the square root of the wetted surface ($\sqrt{S}$). This is the area of the heat sink which is in touch with the air flow (fig 16).

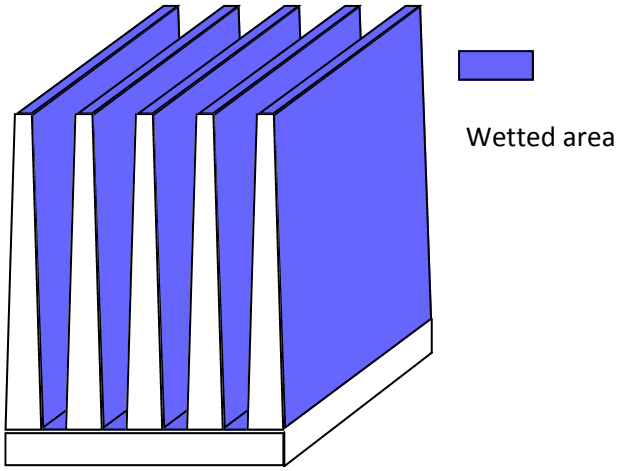

Fig. 16 Wetted area (S)

Therefore, the convection coefficient can be obtained from:

$$h = \frac{Nu_{\sqrt{S}} \cdot k_f}{\sqrt{S}} \qquad (52)$$

Where $Nu_{\sqrt{S}}$ is the Nusselt number with $\sqrt{S}$ as a characteristic length (m), and k_f the fluid conductivity (W/mK).

There is a cuboid associated to the heat sink. This cuboid has the dimensions of HxwxL.

The Nusselt number is defined by:

$$Nu_{\sqrt{S}} = Nu_{\sqrt{S}}^{\infty} + f(Pr)G_{\sqrt{S}}Ra_{\sqrt{S}}^{0.25} \qquad (53)$$

Where $Nu_{\sqrt{S}}^{\infty}$ is the diffusive limit for a cuboid, $f(Pr)$is the "universal" Prandtl number function, $G_{\sqrt{S}}$ is the body-gravity function, and $Ra_{\sqrt{S}}$ is the Rayleigh number with $\sqrt{S}$ as a characteristic length (m).

Therefore, the Rayleigh is defined as:

$$Ra_{\sqrt{S}} = Gr \cdot Pr = \frac{Pr \cdot g \cdot \beta \cdot (T_s - T_\infty) \cdot \sqrt{S}^3}{\nu^2} \qquad (54)$$

All proprieties are evaluated at the average fluid temperature T_m. In most problems, the temperature can be calculated as:

$$T_m = \frac{T_s + T_\infty}{2} \qquad (55)$$

Where T_s is the fin temperature and $T_\infty$is the ambient temperature (K)

The diffusive limit $Nu_{\sqrt{S}}^{\infty}$ is defined as:

$$Nu_{\sqrt{S}}^{\infty} = \frac{3.192 + 1.868(H/L)^{0.76}}{\sqrt{1 + 1.189(H/L)}} \quad (56)$$

Where L, H, W are the dimensions of the cuboid associated to the heat sink (m) defined in Fig. 15.

The "universal" Prandtl function is defined as:

$$f(Pr) = \frac{0.670}{[1 + (0.5/Pr)^{9/16}]^{4/9}} \quad (57)$$

Where *Pr* is the Prandtl number.

The body gravity function can be written as:

$$G_{\sqrt{S}} = 2^{1/8}\left[\frac{H \cdot \Lambda^2}{(n_a \cdot t_a \cdot L + t_a \cdot W + H \cdot \Lambda)^{3/2}}\right]^{1/4} \quad (58)$$

Where:

$$t_a = \frac{t_{af} + t_{ab}}{2}$$

t_a is the average fin thickness (m), t_{af} is the tip fin thickness and t_{ab} is the base fin thickness (m), and:

$$\Lambda = n_a H + t_p + W$$

Where n_a is the number of fins of the heat sink. The other geometric parameters are defined in fig 15.

5.2.2.2 Work of Bilitzky

The studies of Bilitzky [4] (1986) improved the work [5] of Van de Pol and Tierney (1973). Both studies are based on Elenbaas correlation for parallel plate arrays. The Bilitzky and Tierney expressions include aspect ratio factors for a better fitting of U channel profiles. In these correlations, the characteristic length is the hydraulic radius.

$$r = 2\frac{A}{P} \quad (59)$$

Where *A* is the channel cross sectional area (m^2) and *P* is the channel wetted perimeter (m^2).

The convection coefficient is defined as:

$$h = \frac{Nu_r \cdot k_f}{r} \quad (60)$$

Where k_f is the fluid conductivity (W/mK).

The Nusselt number, according to Van de Pol work can be expressed as:

$$Nu_r = \frac{El_r}{\psi}\left[1 - e^{-\psi\left(\frac{0.5}{El_r}\right)^{0.75}}\right] \tag{61}$$

Where ψ is the Van de Pol geometric parameter and El_r is the Elenbaas number. The Bilitzky ψ_B geometric parameter can replace the Van de Pol ones.

The Bilitzky ψ_B parameter is calculated by:

$$\psi_B = \frac{24\Lambda_1}{\left[\left(1 + \frac{a}{2}\right)(1 + \Lambda_2\Lambda_3)\right]^2} \tag{52}$$

$$a = \frac{s_m}{H}$$

$$B = 1.25\left(1 + \frac{s_m}{2H}\right)$$

$$\Lambda_1 = 1 - 0.483e^{-\frac{0.17}{a}}$$

$$\Lambda_2 = 1 - e^{-0.83a}$$

$$\Lambda_3 = 9.14a^{0.5}e^{-B} - 0.61$$

Where S_m is the average inter-fin spacing and H is the fin height.

In channel problems, the Elenbaas number with r as a characteristic length is defined as:

$$El_r = Ra_r\frac{r}{L} \tag{63}$$

Where Ra_r is the Rayleigh number with r as a characteristic length (m) and L is the heat sink length (m).

The Rayleigh number is calculated by:

$$Ra_r = \frac{g \cdot \beta \cdot (T_s - T_\infty) \cdot r^3}{\nu^2}Pr \tag{64}$$

All fluid proprieties have to be calculated at the surface temperature T_s, with the exception of β, which is taken at the average fluid temperature T_m using the equation (55)

Finally, the convection coefficient h can be calculated from equation (60).

5.3 Convection coefficient in forced convection

The forced convection is a type of heat transfer in which fluid motion is generated by an external source (like a pump, fan, suction device, etc.). The convection coefficients are remarkably higher, up to x10 times, so the heat sinks dimensions can be notably reduced.

The convection coefficient is taken from the model proposed by P. Teertstra in his article [6] published in 2000. It can be written as:

$$h = \frac{Nu \cdot k_f}{s_m} \tag{65}$$

Where *Nu* is the Nusselt number, k_f is the fluid conductivity and s_m inter fin space as characteristic linear dimension (m).

In parallel plate channels the flux is found developing conditions, fully developed conditions or simultaneously in both conditions. Churchill and Usagi [7] proposed a composite solution.

$$Nu = \left[\left(Nu_{fd}\right)^{-n} + \left(Nu_{dev}\right)^{-n}\right]^{-1/n} \tag{66}$$

Where *Nu* is the composite Nusselt solution, Nu_{fd} is the asymptotic solution for a fully developed flow, Nu_{dev} is the asymptotic solution for a developing flow and *n* is a combination parameter which depends on the model. In the model proposed by Teertstra, n has the value of 3.

All fluid temperatures will be calculated at film temperature T_f (K). The film temperature is the average temperature of the boundary layer.

$$T_f = \frac{T_s + T_\infty}{2} \tag{67}$$

Where T_s is the surface temperature and T_∞ (K) is the ambient temperature (K).

The Nusselt Number for the fully developed flow asymptote can be expressed as:

$$Nu_{fd} = \frac{1}{2}\frac{s_m}{L} Re_{s_m} Pr \tag{68}$$

The Nusselt number for the developing flow asymptote is defined as:

$$Nu_{dev} = 0.664 \cdot \left(\frac{s_m}{L} Re_{s_m}\right)^{0.5} Pr^{1/3} \left(1 + \frac{3.65}{\left(\frac{s_m}{L} Re_{s_m}\right)^{0.5}}\right)^{0.5} \tag{69}$$

Where s_m is the average inter fin space, *Pr* is the Prandtl number defined in (45), Re_{sm} is the Reynolds number defined in (43) with s_m as a characteristic linear dimension (m) and *L* is the heat sink length (m).

6 Simple algorithm

The objective of this algorithm is to know the junction temperature T_{jun} for a given heat sink and working conditions.

The general expression used to know the power dissipated by a heat sink can be written as:

$$q = \frac{T_{jun} - T_{amb}}{R_{sa} + R_{cs} + R_{jc}} = \frac{T_{jun} - T_{amb}}{R_{bf} + R_{sp} + R_{fa} + R_{cs} + R_{jc}} \tag{70}$$

Where:

T_{jun}	Junction temperature (K)	The maximum junction temperature is given by the manufacturer
T_{amb}	Ambient temperature (K)	Is the ambient working temperature. To analyze critical situations, a maximum ambient temperature is required.
R_{cs}	Case-Sink resistance (C/W)	It depends on the assembly method, the sink and device geometry, the surface roughness and the thermal grease type. It can be neglected in most cases.
R_{jc}	Junction case resistance (C/W)	It is usually given by the device manufacturer.
R_{sa}	Sink ambient resistance (C/W)	It is divided into several resistances.
R_{bf}	Plate conduction resistance (C/W)	It depends on geometric parameters and the plate conductivity.
R_{sp}	Spreading resistance (C/W)	It depends on geometric parameters and plate conductivity. In other models also depends on the convection coefficient.
R_{fa}	Fin ambient resistance (C/W)	It depends on geometric parameters and fluid proprieties. These fluid proprieties also depend on the sinks surface temperature.

The junction temperature can be written as:

$$T_{jun} = q\left(R_{bf} + R_{sp} + R_{fa} + R_{cs} + R_{jc}\right) + T_{amb} \tag{71}$$

All parameters can be deduced directly from the sink geometry and its proprieties, except the R_{fa}, which also depends on the sink surface temperature T_s.

Therefore, determining the surface temperature is a requirement to know the junction temperature. However, the surface temperature is implicit in model functions and is needed an iteration process in order to know this temperature.

So, for R_{fa}, the general equation can be written as:

$$q = \left(h_c(T_s) + h_r(T_s)\right) \cdot \left(A_p + \eta(T_s) \cdot A_f\right) \cdot (T_s - T_{amb}) = \frac{T_s - T_{amb}}{R_{fa}(T_s)} \tag{72}$$

Assuming:

- All heat transfer rate q occurs in fin-side plate surface.
- The T_s temperature will be taken as the average surface temperature.
- The convection coefficient is constant along the fins surface.

- The radiation equivalent coefficient is constant along the fins surface.

At this point, the iteration process can be defined as:

T_{s1}=80ºC

T_s=0ºC

q=P (the total heat power from the device)

While $|T_{s1} - T_s|>0.01$

$T_s = T_{s1}$

Calculate h_c for T_s from any model proposed.

Calculate h_r for T_s from the model proposed.

Calculate h_{tot} as $h_{tot} = h_c + h_r$

Calculate η for h_{tot} from the model proposed.

Calculate R_{fa} as $R_{fa} = 1/\left(h_{tot} \cdot \left(A_p + \eta A_f\right)\right)$

Calculate T_{s1} as $T_{s1} = q \cdot R_{fa} + T_{amb}$

End

$T_s = T_{s1}$

Calculate R_{fa} by $R_{fa} = (T_s - T_{amb})/q$

The other resistances can be directly calculated from the explicit equations defined in the previous sections and the data given by the manufacturer.

Using equation (68), T_{jun} is determined.

Finally T_{jun} is compared with the max junction temperature T_{junmax} value given by the manufacturer in order to know the feasibility of the heat sink design.

7 Multiple heat source model

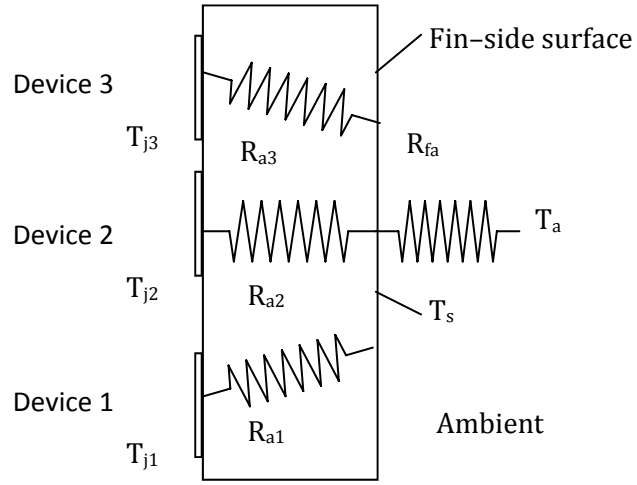

Fig. 17 multiple heat sources resistances

In heat sinks with multiple heat sources, the lineal resistance method becomes useless. The reason is that are induced multiple asymmetric resistances inside the plate (Fig.16).

An unfeasible case is exposed below.

An average surface temperature T_s is assumed and the resistance equation can be written as:

$$q_1 = \frac{T_{jun1} - T_s}{R_{a1}} \tag{73}$$

Where T_{jun1} is the junction temperature of the device 1 (K), q_1 is the heat transfer rate from the device 1 (W), R_{a1} is the plate resistance associate to heat flux1 (C/W).

In some configurations, the average surface temperature T_s might be higher than a junction temperature T_n. Then, for an eventual heat source device (q_n>0), the resistance R_{an}, would be negative. This is fiscally impossible, so the lineal resistance method is rejected as a method for multiple heat sources.

The solution is proposed in the article of Y. S. Muzychka, J. R. Culham, M. M. Yovanovich [8]. Their model solves mathematically the multiple eccentric heat sources question.

From the Laplace equation:

$$\nabla^2 \cdot \mathrm{T} = \frac{\partial^2 \mathrm{T}}{\partial \mathrm{x}^2} + \frac{\partial^2 \mathrm{T}}{\partial \mathrm{y}^2} + \frac{\partial^2 \mathrm{T}}{\partial \mathrm{z}^2} = 0 \tag{74}$$

Restricting:

Conduction at source surface $A_s=L_d x w_d$ $$\left.\frac{\partial T}{\partial z}\right|_{z=0} = -\frac{(P_d/A_s)}{k_1}$$

Plate thickness isolated $$\left.\frac{\partial T}{\partial z}\right|_{x=0,w} = 0$$

$$\left.\frac{\partial T}{\partial z}\right|_{y=0,L} = 0$$

Source- side plate surafce isolated $$\left.\frac{\partial T}{\partial z}\right|_{z=0} = 0$$

Convection on the fin-side plate surface $$\left.\frac{\partial T}{\partial z}\right|_{z=t_p} = -\frac{h_m}{k}\left(T(x,y,t_p) - T_{amb}\right)$$

Where h_m is modified convection coefficient, expressed as:

$$h_m = \frac{\left(A_p + \eta \cdot A_f\right) \cdot h_{total}}{w \cdot L} \tag{75}$$

Where A_p is the primary surface, A_f is the fin surface (Fig. 5), η is the fin efficiency, w is the sink width and L is the sink length (Fig. 15).

To find the solution of equation (71) is useful applying this equality:

$$\bar{\theta}_j = \bar{T}j - T_{amb} = \sum_{i=1}^{N} \bar{\theta}_{i,j} \tag{76}$$

Where $\bar{T}j$ is the average temperature of the heat source j surface, $\bar{\theta}_{i,j}$ is the temperature difference between the surface of the source j and the ambient due to the heat source i.

$\bar{\theta}_{ij}$ can be expressed as:

$$\begin{aligned}
&\bar{\theta}_{ij} = \\
&= A_0^i \\
&+ 2\sum_{m=1}^{\infty} A_m^i \frac{\cos\left(\lambda_m x_{c,j}\right) \sin\left(\lambda_m w_{d,j}/2\right)}{\lambda_m w_{d,j}} \\
&+ 2\sum_{n=1}^{\infty} A_n^i \frac{\cos\left(\delta_n y_{d,j}\right) \sin\left(\delta_n L_{d,j}/2\right)}{\delta_n L_{d,j}} \\
&+ 4\sum_{m=1}^{\infty}\sum_{n=1}^{\infty} A_{mn}^i \frac{\cos\left(\delta_n y_{dj}\right) \sin\left(\delta_n L_{dj}/2\right) \cos\left(\lambda_m x_{cj}\right) \sin\left(\lambda_m w_{dj}/2\right)}{\lambda_m w_{dj} \delta_n L_{dj}}
\end{aligned} \tag{77}$$

Where:

$$\lambda_m = m \cdot \pi / w, \qquad \delta_n = n \cdot \pi / L \quad \text{i} \quad \beta_{m,n} = \sqrt{{\lambda_m}^2 + {\delta_n}^2}$$

$$A_1^i = \frac{P_d^i}{L w_d^i k \lambda_m \emptyset(\lambda_m)} \frac{\int_{x_d^i - \frac{w_d^i}{2}}^{x_d^i + \frac{w_d^i}{2}} \cos\left(\lambda_m x\right) dx}{\int_0^w \cos^2\left(\lambda_m x\right) dx}$$

$$A_m^i = \frac{2P_d^i \left[\sin\left(\frac{\left(2x_d^i + w_d^i\right)}{2}\lambda_m\right) - \sin\left(\frac{\left(2x_d^i - w_d^i\right)}{2}\lambda_m\right)\right]}{wLw_d^i k {\lambda_m}^2 \emptyset(\lambda_m)}$$

$$A_2^i = \frac{P_d^i}{w L_d^i k \delta_n \emptyset(\delta_n)} \frac{\int_{y_d^i - \frac{L_d^i}{2}}^{y_d^i + \frac{L_d^i}{2}} \cos\left(\delta_n y\right) dy}{\int_0^L \cos^2(\delta_n y)\, dy}$$

$$A_n^i = \frac{2P_d^i\left[\sin\left(\frac{\left(2y_d^i + L_d^i\right)}{2}\delta_n\right) - \sin\left(\frac{\left(2y_d^i - L_d^i\right)}{2}\delta_n\right)\right]}{wLL_d^i k{\delta_n}^2 \emptyset(\delta_n)}$$

$$A_3^i = \frac{P_d^i}{w_d^i L_d^i k\beta_{m,n}\emptyset(\beta_{m,n})} \frac{\int_{y_d^i-\frac{L_d^i}{2}}^{y_d^i+\frac{L_d^i}{2}} \int_{x_d^i-\frac{w_d^i}{2}}^{x_d^i+\frac{w_d^i}{2}} \cos(\lambda_m x)\cos(\delta_n y)dxdy}{\int_0^L \int_0^w \cos^2(\lambda_m x)\cos^2(\delta_n y)\,dxdy}$$

$$A_{mn}^i = \frac{16P_d^i cos(\lambda_m x_d^i) sin(\lambda_m w_d^i/2) cos(\delta_n y_d^i) sin(\delta_n L_d^i/2)}{wLL_d^i w_d^i k\beta_{m,n}\lambda_m\delta_n\emptyset(\beta_{m,n})}$$

$$\emptyset(\zeta) = \frac{\zeta\sinh(\zeta\cdot t_p) + (h_m/k)\cosh(\zeta\cdot t_p)}{\zeta\cosh(\zeta\cdot t_p) + (h_m/k)\sinh(\zeta\cdot t_p)}$$

$$A_0^i = \frac{P_d^i}{wL}\left(\frac{t_p}{k} + \frac{1}{h_m}\right)$$

Where *k* is the plate conductivity (W/mK), P_d^i is the power of the device i, x_d^i , y_d^i, L_d^i , w_d^i , L, w are geometric parameters for de device i (fig 19).

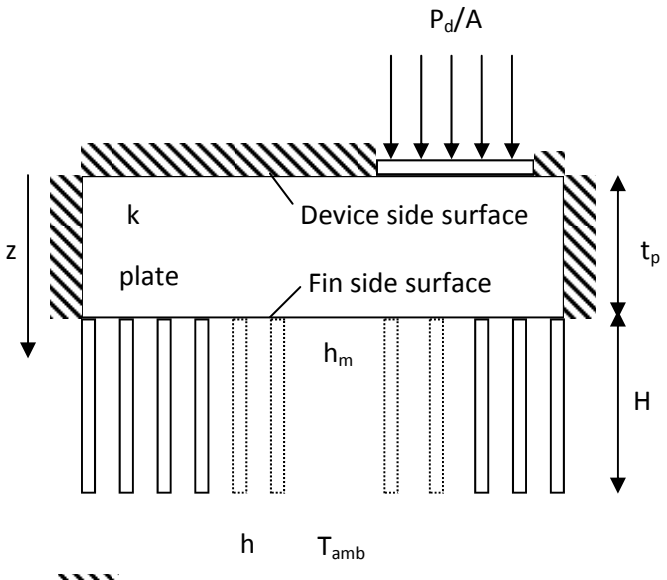

Fig. 18 Heat sink insulating zone

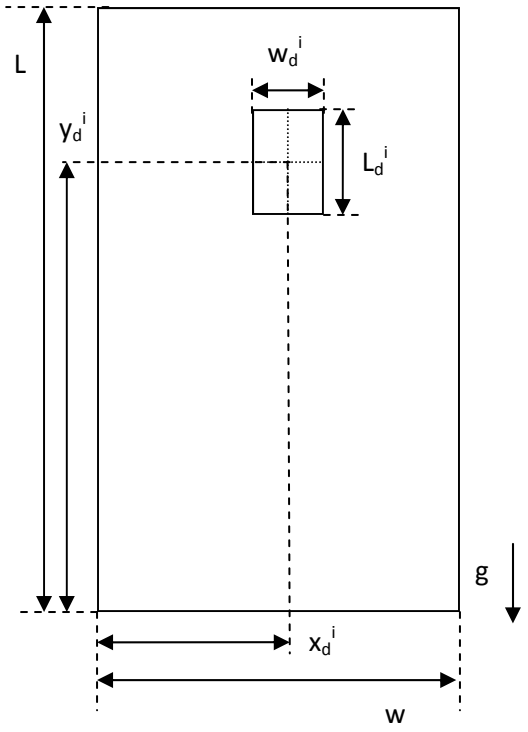

Fig. 19 Heat sink device distribution parameters

8 Multiple heat sources algorithm

The objective of this algorithm is to know the junction temperatures for a given sink and working conditions. In this case, several heat sources can be added in any distribution.

In order to know the junction temperatures of each device, the multiple heat source model defined in the previous section will be used.

Assumptions

- All heat transfer rate q occurs in fin-side plate surface. (Fig. 18)
- The T_s temperature will be taken as the average surface temperature.
- The convection coefficient is constant along the fins surface.
- The radiation equivalent coefficient is constant along the fins surface. This assumption does not take into account that the radiation is higher in the external fins than the internal fins.
- The temperature of the sink surface in contact with each device will be taken as an average of the temperature of all contact surface (Fig. 20)
- The number of devices is N.

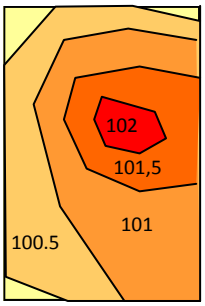

Heat sink device-surface

Fig. 20 Device temperature distribution sample

From these assumptions, the algorithm is developed bellow:

T_{s1}=80ºC

Ts=0ºC

$q=P_1+P_2+...+P_N$ (Total heat power generated from devices)

While $|T_{s1} - T_s|>0.01$

$T_s = T_{s1}$

Calculate h_c for T_s from any model proposed.

Calculate h_r for T_s from the model proposed.

Calculate h_{tot} as $h_{tot} = h_c + h_r$

Calculate η for h_{tot} from the model proposed.

Calculate R_{fa} as $R_{fa} = 1/\left(h_{tot} \cdot \left(A_p + \eta A_f\right)\right)$

Calculate T_{s1} as $T_{s1} = q \cdot R_{fa} + T_{amb}$

End

$T_s = T_{s1}$

Calculate $\bar{\theta}_{ij}$ matrix $\begin{pmatrix} \bar{\theta}_{1,1} & \cdots & \bar{\theta}_{1,N} \\ \vdots & \ddots & \vdots \\ \bar{\theta}_{N,1} & \cdots & \bar{\theta}_{N,N} \end{pmatrix}$

Using the equation (76), the total temperature difference $\bar{\theta}_j$ between the device zone and the ambient for the heat source j is: $\bar{\theta}_j = \bar{T}j - T_{amb} = \sum_{i=1}^{N} \bar{\theta}_{i,j}$. $\bar{\theta}_j$ can also be obtained from the addition of the column j.

Calculate $\bar{T}j$ from $\bar{T}j = \bar{\theta}_j + T_{amb}$.

From the average temperature of the source j, the junction temperature is calculated from: $T_{jun,j} = P_j\left(R_{jc,j} + R_{cs,j}\right) + T_{amb}$

Compare the $T_{jun,j}$ for the given max junction temperature for the device $T_{junmaxj}$.

9 Computation results

Natural convection has been tested in order to know the precision of the algorithms proposed. There is available in the net a free online modeling tool, R-tools [9] , offered by Mersen. This program is based on an advanced three-dimensional numerical model, and there are many sink profiles available.

The multiple heat source algorithm has included the models of Bilitzky and Yovanivich for natural convection. Moreover, the Bilitzky model has been analyzed with the fluid proprieties evaluated at the wall temperature and at the boundary temperature. The Van de Pol article, which the Bilitzky model is based, holds the wall temperature as the reference temperature to calculating most fluid proprieties. Anyway, it can be an experiment to verify it.

It has been analyzed 45 profiles of 102. The profiles excluded are either those are not available in R-tools or are not able to be parameterized because its geometry.

Each profile has been tested at length of 50%, 100% 150% and 200% of its width. Then, it has been 180 tests, 4 per profile.

Each simulation had got one heat source, which has occupied totally the sink surface. The source heat generation rate has been estimated for each simulation in order to have junction temperatures from 90º C to 140 ºC. These values are usually the maximum junction temperature given by the manufacturers.

Then, the algorithm model and the R-tools results have been compared. The results are presented in the appendix 1.

9.1 Discussion of the results

The admissible error has been set up at 15%. The appendix 1 shows the relative error of each model respect the r-tools results.

The average error for the three proposed models is exposed below:

	Average	Median
Bilitzky Wall temperature model	10,4%	8,5%
Bilitzky boundary temperature model	10,5%	8,7%
Yovanovich model	20,5%	15,5%

Table 1 Error comparison

These results do not reveal an important average error difference between both Bilitzky models. However, there is a considerable difference for some individual tests results. For certain profiles, the difference between both Bilitzky models is as high as 10%.

Each profile has a model which approach better to r-tool results. Of 45 profiles, the average error for the 4 test that each profile is subjected is minimal in Bilitzky-Wall model 20 times, in Bilitzky-Boundary model 13 times and in Yovanovich model 12 times. So, there is not an obvious winner.

If the better model for each individual profile was used, the average error would drop to 8.12% and the median would fall to 6.05%.

In conclusion, a mixed model could improve the precision.

There is a remarkably correlation between the error from a given model and some geometric parameters.

Some of these parameters are:

- $s_m/_{wa}$: is the relation between the average inter-fin spacing (s_m) and the wetted area (wa). This parameter is well correlated to both Bilitzky models as showed in fig 21 and fig 22.
- s_m: is the average inter-fin spacing. It is strongly correlated with the error of Yovanovich model as shows fig 23.

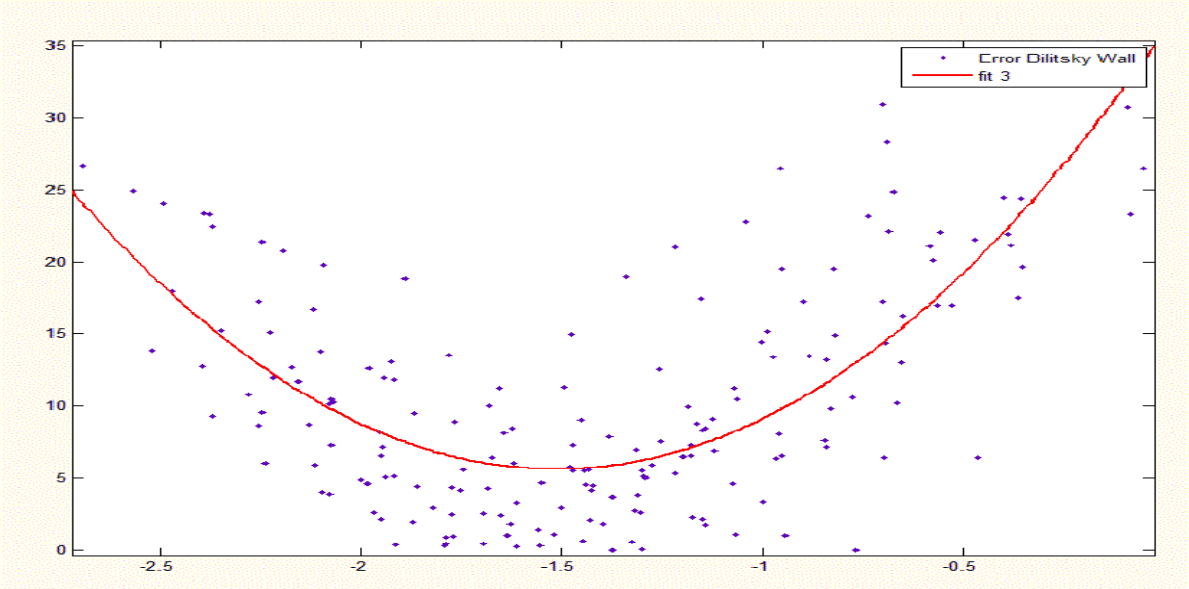

Fig. 21. Error Bilitzky wall vs LOG10(s_m/wa). R^2=0.528

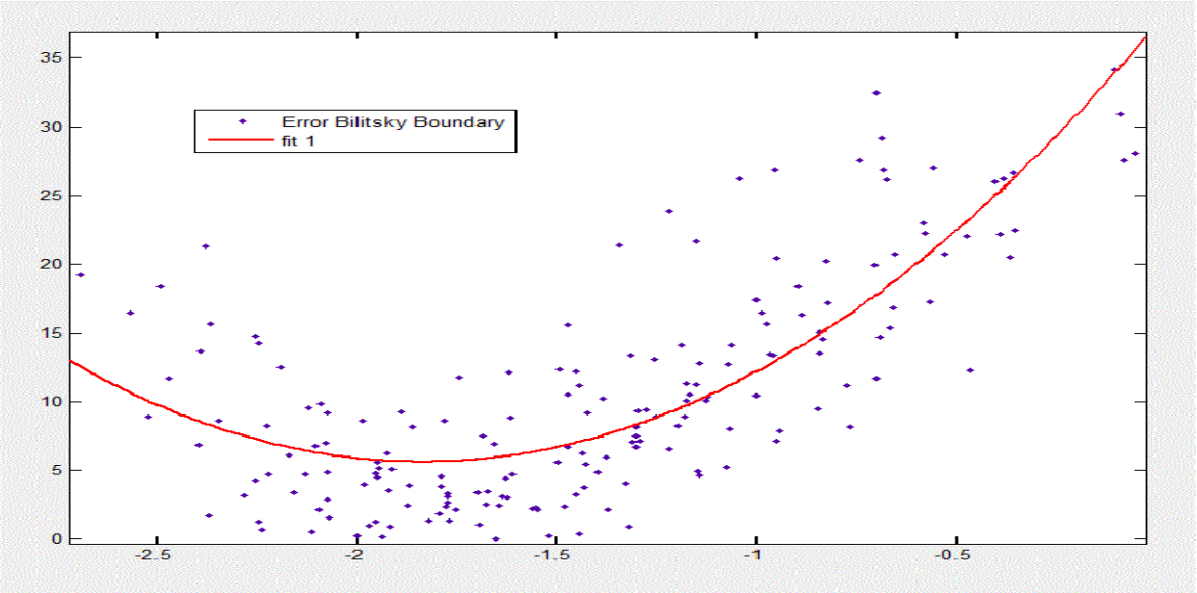

Fig. 22 Error Bilitzky Boundary vs LOG10(s_m/wa). R^2=0.625

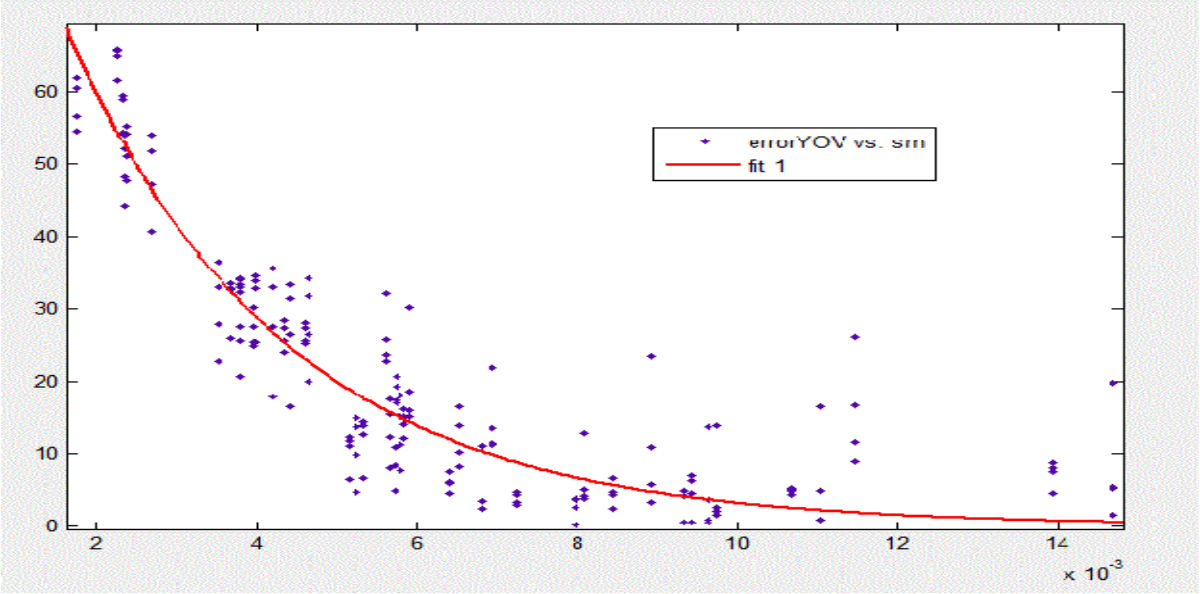

Fig. 23 Error Yovanovich vs s_m. R^2=0.859

There is available in Matlab two applications, curve fitting tool and surface fitting tool, which may help to identify new correlations.

10 Optimization process

An optimization process leads to find a set of parameters which minimize or maximize a function, satisfying a set of constraints.

The optimization in heat sinks can minimize the volume, the price, the length or the weight for a given working conditions.

An optimization is often developed as an iteration process ruled by an algorithm.

The proposed convection model can be optimized, admitting a precision error. However, the precision can be remarkably improved adding constraints to allow the algorithm work in favorable range of parameters.

For example, if the error in Yovanovich model is lower at large inter-fin spacing values (fig 22). A hypothetical constraint limiting the minimum inter-fin space could be added in order to work in propitious ranges of values where the error is statistically notably lower.

There are several algorithms available. In the next section is the genetic algorithm.

10.1 The genetic algorithm

The genetic algorithm is based on biologic evolution. Heat sinks have several parameters (Length, fin height, width…) which determine the sink performance. These parameters (P1, P2…) define an individual and are bounded by upper and lower limits, which are predetermined by physical, manufacture or model limitations (fig 24).

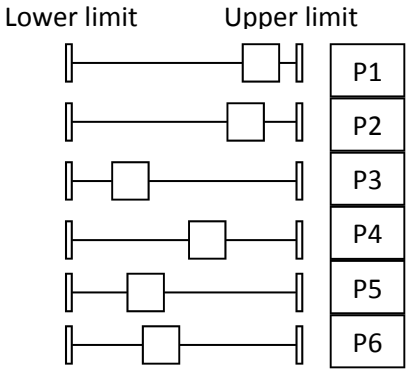

Fig. 24 Algorithm parameters

There is also a set of constraints. These constraints involve more than one parameter and must be evaluated after defining an individual.

The constraints may include:

- Geometric constraints: the devices must be placed in the sink surface, and cannot be superimposed.
- Manufacturing constraints: the heat sinks are usually made by extrusion. In extrusion, the aspect ratio (the relationship between the spacing and the height of the fins) and the minimum fin thickness are limited. The manufacturing methods have been notably improved during the 90's and 00's. Actually, most manufacturers offer aspect ratios up to 1:10 and minimum fin thickness of 1mm [10].
- Temperature constraints: The junction temperature cannot exceed the maximum junction temperature given by the manufacturer. In addition, some standards in industry can restrict the temperature of the sink surface.

Finally there is as objective function. This function specifies the variable (volume, length, weight…) which is wanted to be minimized or maximized.

The algorithm steps are explained bellow.

1. Creation of an individual who satisfies all constraints.

2. Random creation of the first generation. All individuals are composed from the original individual.

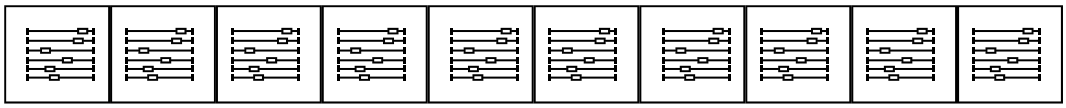

3. Ordering the individuals. Every individual has an objective function value. Moreover, they may or may not satisfy the constraints. They are ordered from best to worst. Those that may not satisfy the constraints obtain automatically a very high number as objective function value.

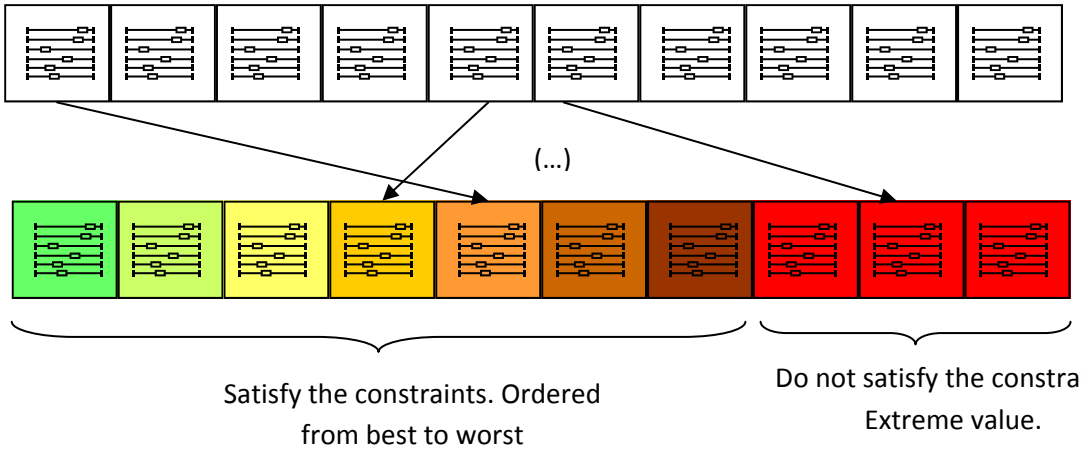

4. Crossover and mutation. The next generation is created either from the crossover of the previous generation, either from the mutation of some parameters. Each algorithm has a mutation ratio fixed by the user.

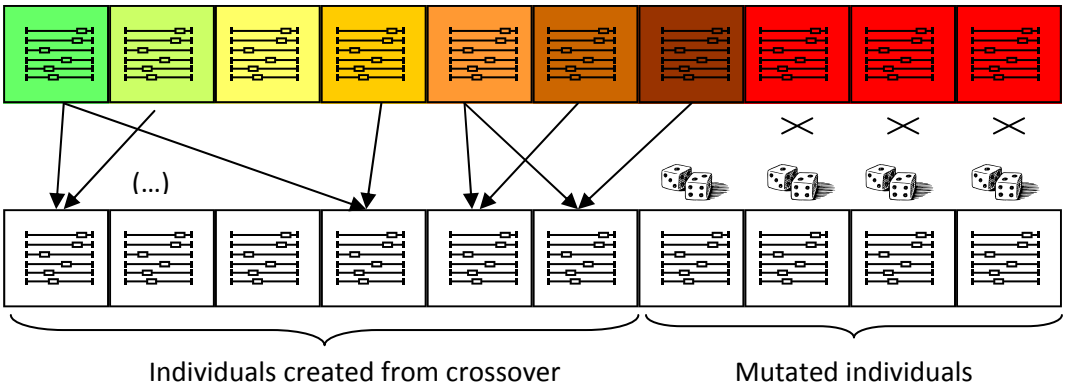

5. Ordering the individuals as 3. Iteration process.

6. The algorithm finishes either after a certain number of iterations, either after observing no changes in the best individual (the fist after ordering) during a fixed number of iterations.

10.2 Optimization sample for heat sinks

The multiple heat sources algorithm has been tested in Matlab. Each individual is composed by 3 continuous parameters (Fig. 25):

- L: Length
- D_{PD}: distance between pair of devices
- D_{LD}: distance between the lines of devices.

The objective function is the minimum length. The algorithm finishes after 400 generations or when there is not a significant decrease of the objective function after 30 generations.

The algorithm has finished after 203 iterations.

The Fig. 26 shows the evaluation of the objective function along iterations. Notice the quick decrease of the objective function in the first iterations.

The Fig. 27 and Fig. 28 show respectively the variation of the DPD and PLD along iterations. Notice the great variation of both parameters.

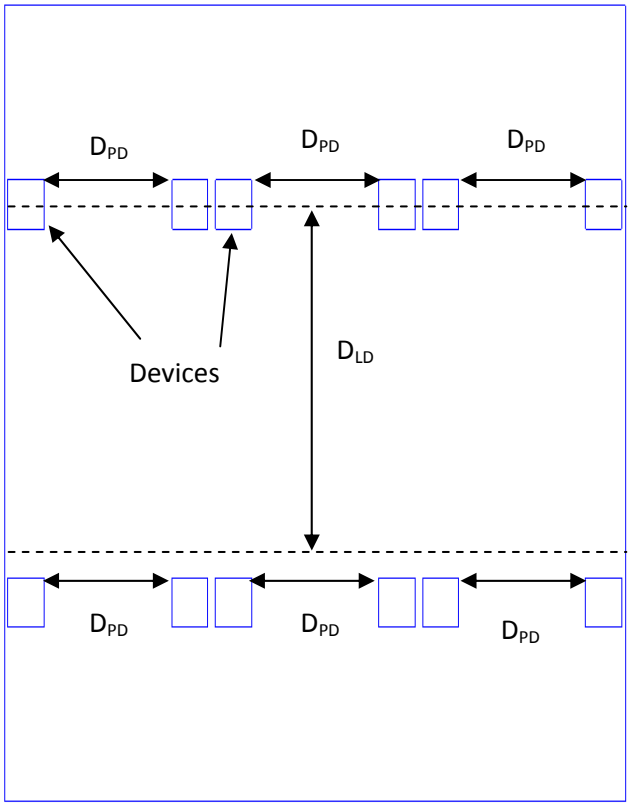

Figure 25 Heat Sink Optimization parameters

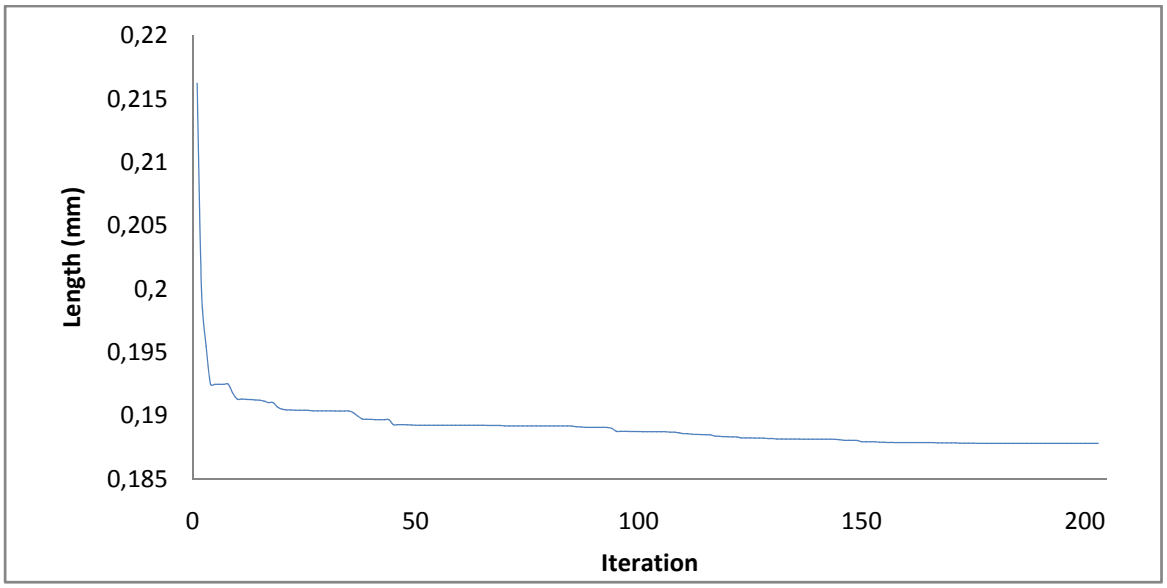

Figure 26 Length variation along iterations

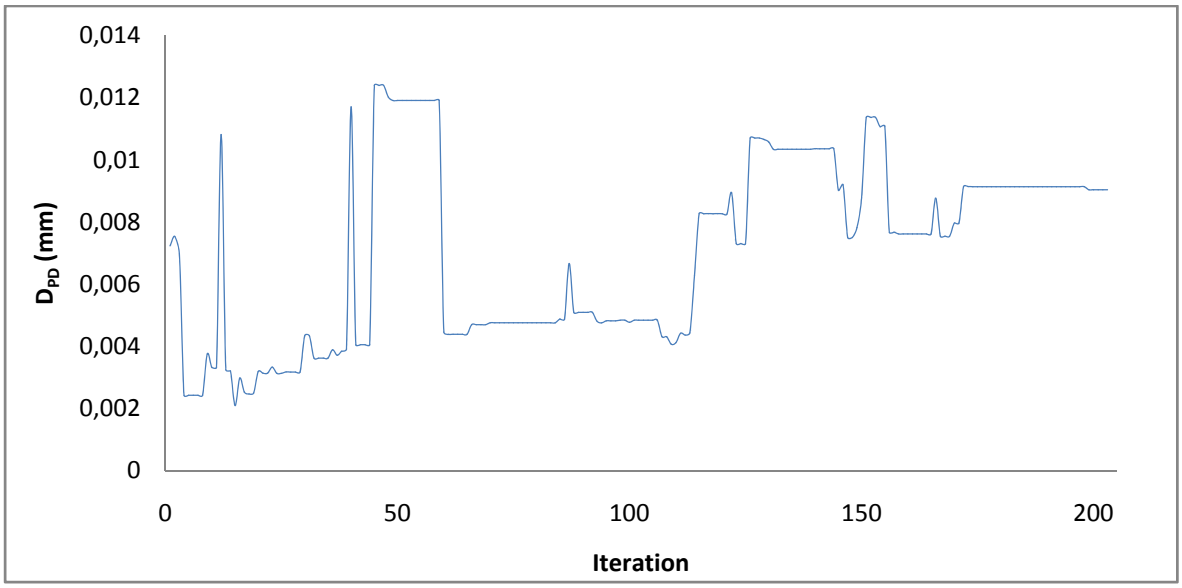

Figure 27 DPD Variation along Iterations

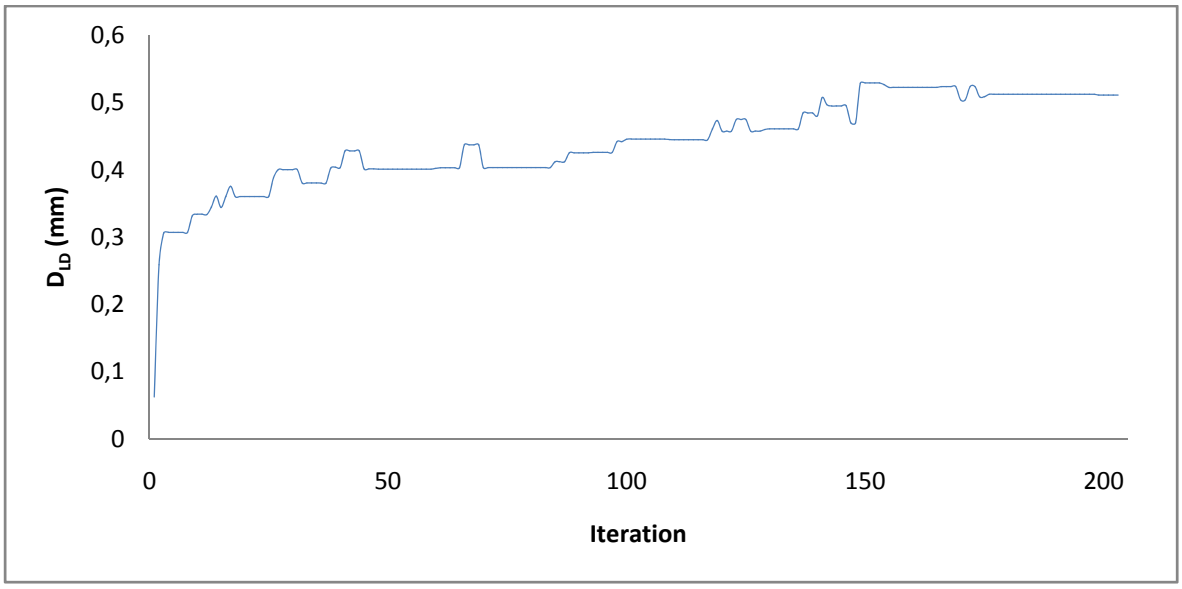

Figure 28 DLD Variation along Iterations

11 Conclusion

Good agreement obtained in comparisons between the R-tool data and the algorithm proposed, reveal the viability of using the multiple heat source algorithm as a tool for heat sinks.

Three sample applications for this algorithm are exposed bellow:

- Determining the feasibility of a heat-sink device assembly.
- Optimizing heat sink geometry for a specific application.
- Tracing Resistance-Length curves for a given profile.

The 180 tests of 45 profiles give significant information about the behaviour of the algorithm. The analysis of this behaviour is a key for improving future models. In this document, the error has been correlated to two parameters, nevertheless a new study could find easily new correlations. Limiting the actuation range of the proposed algorithm may lead to a precision increase.

For a meticulous future work, the errors for natural convection, radiation and spreading phenomenon models must be analyzed and parameterized separately.

The convection models must be compared with experimental data and the results of computational fluid dynamics software such as Fluent or as Floworks. That could help to analyse thoroughly the conduct of each model in function of particular parameters or relations.

The proposed radiation model is an approximation in which the error depends on geometric relations. Working with real view factors may lead to improve the radiation heat ratio agreement.

Afterwards, mixing models or even creating new ones could make possible more performing algorithms.

However, the surface temperature will always be an inconvenient since it is not a constant value. It changes along the plate surface and along the fin surfaces. Long heat sinks tend to have a great variance in their surface temperature. The air proprieties change as it is heated along the sink. The fluid heat absorption capacity decreases and the highest zones of the heat sinks are less cooled.

This creates asymmetries that cannot be easily simulated by analytical methods. A simple 3D model where only the plate was meshed could be a good way to remarkably improve the precision, without wasting too much computational sources.

By using analytically approaches, other types of shapes could be also deduced. Some heat sink profiles are very branched, but there are linear transformations available that can facilitate the modelling. It is also necessary to develop natural convection models for V channels to determine the convection coefficient for these branched sinks.

12 References

[1] Shabany, Younes (2008). “Simplified correlations for radiation heat transfer rate in plate fin heat sinks.” http://www.electronics-cooling.com/2008/08/

[2] Elenbaas, W (1942). “Heat dissipation of parallel plates by free convection”. Physica Vol IX, No 1. 1-28.

[3] J. Culham, M Yovanovich and Seri Lee (1995). Thermal modeling of isothermal cuboids and rectangular heat sinks cooled by natural convection”. IEEE Transactions on components, packaging, and manufacturing technology- part A. Vol. 19, NO 3. September 1995.

[4] Bilitzky, A. (1986). The Effect of Geometry on Heat Transfer by Free Convection from a Fin Array, M.S. thesis, Department of Mechanical Engineering, Ben-Gurion University of the Negev, Beer Sheva, Israel.

[5] Van de Pol, D. W. and Tierney, J. K. (1973). Free Convection Nusselt Number for Vertical U-Shaped Channels, J. Heat Transfer, 87, 439.

[6] P. Teertstra, M.M. Yovanovich and J.R. Culham. “Analytical forced convection modeling of Plate fin heat sinks” Journal of electronics manufacturing, Vol. 10, No. 4 (2000) pp. 253 261.

[7] Churchill, S. W. and Usagi, R., “A general expression for the correlation of rates of transfer and other phenomenon”. A.I.Ch.E. Journal, Vol. 18, pp. 1121 – 1128. 1972

[8] Y. S. Muzychka, J. R. Culham, M. M. Yovanovich (2008). Thermal Spreading Resistance of Eccentric Heat Sources on Rectangular Flux Channels. Journal of Electronic Packaging JUNE 2003, Vol. 125.

[9] http://www.r-tools.com/

[10] Kuzmin, G. (2004) Innovative heat sink enables hot uplinks. Power electronics technology, pp 14-20. November 2004.

Appendix 1. Profiles and computation results

Full Surface Heat Transfer		Aluminum Extrusion Profiles Ferraz Shawmut / Mersen	r-theta results			Junction temperature algorithm Results			% ERROR		
			Length (mm)	Heat (W)	T-junction (C)	Yovanovich (C)	Bil. Boundary (C)	Bil. Wall (C)	Yovanovich	Bil. boundary	Bil. wall
Code	66171	66171 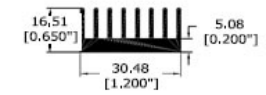	15,2	3	129	88,4	102,1	106,3	41,2%	27,5%	23,3%
Width (mm)	30,48		30,5	4	124	79,6	99,7	104,4	47,4%	26,2%	21,2%
Height (mm)	16,51		45,7	5	127	76,8	100,9	105,8	51,9%	27,0%	22,0%
fins	8		61	6	129	75,6	102,6	107,3	54,1%	26,9%	22,1%
Code	61080	61080 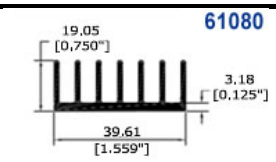	19,8	5	124	97,4	97,5	99,1	28,2%	28,1%	26,5%
Width (mm)	39,61		39,6	10	135	108,6	111,5	114,5	25,3%	22,5%	19,6%
Height (mm)	19,05		59,4	15	145	115,3	121,0	125,3	25,7%	20,7%	17,0%
fins	7		79,2	20	154	120,2	128,4	133,9	27,3%	20,7%	16,3%
Code	61215	61215 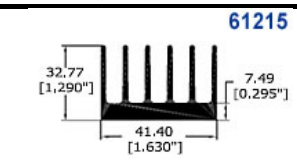	20,7	5	104	79,6	78,4	79,0	32,5%	34,2%	33,4%
Width (mm)	41,4		41,4	10	109	88,8	88,8	90,0	26,0%	26,0%	24,4%
Height (mm)	32,77		62,1	15	115	94,3	95,7	97,5	23,9%	22,2%	20,1%
fins	6		82,8	20	119	98,4	101,0	103,4	22,9%	19,9%	17,2%
Code	66122	66122 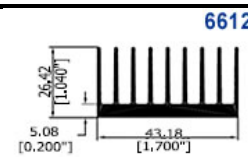	21,6	8	115	93,7	97,8	100,4	25,3%	20,5%	17,5%
Width (mm)	43,18		43,2	16	131	105,4	115,8	121,0	25,7%	15,4%	**10,2%**
Height (mm)	26,42		64,8	24	144	112,5	128,6	135,9	27,7%	**13,5%**	**7,1%**
fins	9		86,4	32	156	117,6	138,7	147,6	30,3%	**13,4%**	**6,4%**
Code	66454	66454 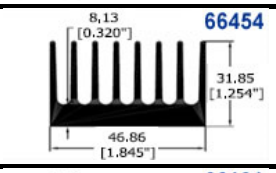	23,4	10	127	99,3	101,4	103,6	28,9%	26,7%	24,4%
Width (mm)	46,86		46,9	15	116	95,4	101,9	105,1	24,3%	16,8%	**13,0%**
Height (mm)	31,85		70,3	20	118	95,2	105,2	109,3	25,9%	**14,6%**	**9,8%**
fins	8		93,7	25	121	95,9	108,8	113,7	27,6%	**13,4%**	**8,1%**
Code	66191	66191 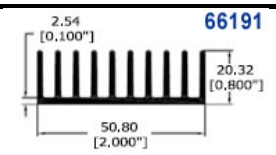	25,4	10	131	107,8	118,4	124,3	22,8%	**12,3%**	**6,5%**
Width (mm)	50,8		50,8	15	130	102,2	122,0	130,1	27,8%	**8,1%**	**0,0%**
Height (mm)	20,32		76,2	20	137	101,6	128,3	137,9	32,9%	**7,8%**	**1,1%**
fins	10		102	25	144	102,1	134,5	144,9	36,5%	**8,0%**	**1,2%**
Code	66408	66408 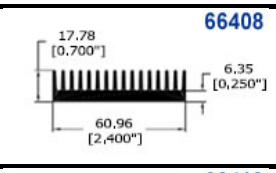	30,5	6	120	70,9	95,4	99,3	54,7%	27,5%	23,2%
Width (mm)	60,96		61	9	122	67,7	98,0	101,2	59,1%	26,2%	22,7%
Height (mm)	17,78		91,4	12	122	67,2	100,0	102,7	59,5%	23,9%	21,0%
fins	16		122	15	121	67,4	101,4	103,7	58,9%	21,4%	19,0%
Code	66419	66419 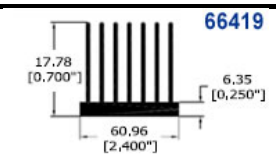	30,5	25	134	102,7	100,5	102,1	30,3%	32,4%	30,9%
Width (mm)	61		61	37,5	115	98,8	99,9	102,4	18,7%	17,4%	**14,5%**
Height (mm)	71,78		91,5	50	112	99,0	102,8	106,1	16,0%	**11,3%**	**7,3%**
fins	7		122	62,5	113	100,1	106,4	110,4	15,0%	**7,4%**	**2,6%**
Code	66280	66280 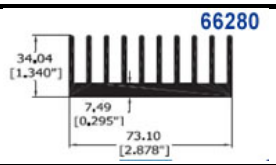	36,6	25	140	116,7	114,5	116,6	21,0%	22,9%	21,1%
Width (mm)	73,1		73,1	37,5	129	111,6	112,4	115,2	17,2%	16,3%	**13,5%**
Height (mm)	34,04		110	50	129	111,3	114,6	118,2	17,4%	**14,1%**	**10,5%**
fins	10		146	62,5	132	112,2	117,7	121,9	19,4%	**14,1%**	**9,9%**

Full Surface Heat Transfer		Aluminum Extrusion Profiles Ferraz Shawmut / Mersen	r-theta results			Junction temperature algorithm Results			% ERROR		
			Length (mm)	Heat (W)	T-junction (C)	Yovanovich (C)	Bil. Boundary (C)	Bil. Wall (C)	Yovanovich	Bil. boundary	Bil. wall
Code	66195	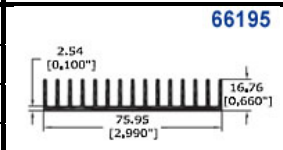	38	15	121	101,9	110,2	114,9	20,8%	**11,7%**	**6,4%**
Width (mm)	75,95		76	22,5	122	96,5	112,3	118,7	27,6%	**10,4%**	**3,4%**
Height (mm)	16,76		114	30	127	95,8	117,2	124,8	32,2%	**10,1%**	**2,3%**
fins	15		152	37,5	130	96,1	122,2	130,5	34,1%	**8,2%**	**0,1%**
Code	66102	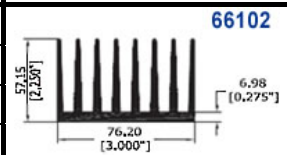	38,1	30	130	108,0	103,8	105,2	22,0%	26,2%	24,8%
Width (mm)	76,2		76,2	45	115	103,7	102,0	103,8	**13,6%**	15,6%	**13,4%**
Height (mm)	57,15		114	60	113	103,9	104,0	106,4	**11,4%**	**11,2%**	**8,3%**
fins	8		152	75	115	105,1	106,8	109,8	**11,5%**	**9,4%**	**6,0%**
Code	66167	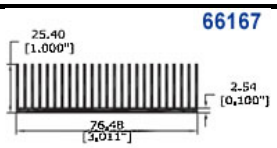	38,2	10	104	58,3	93,8	98,5	61,5%	**13,4%**	**7,0%**
Width (mm)	76,48		76,5	15	107	56,5	100,0	104,2	65,5%	**8,8%**	**3,4%**
Height (mm)	25,4		115	20	107	56,4	104,2	107,8	65,7%	**3,8%**	**1,0%**
fins	25		153	25	106	56,8	107,1	110,3	64,9%	**0,9%**	**5,1%**
Code	62350	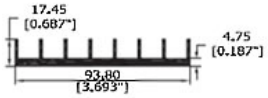	46,9	10	107	86,7	83,3	83,4	26,5%	30,9%	30,7%
Width (mm)	93,8		93,8	15	91,9	81,4	78,2	78,3	16,9%	22,2%	22,0%
Height (mm)	17,75		141	20	86,9	80,3	77,1	77,2	**11,7%**	17,2%	17,0%
fins	8		188	25	85,1	80,1	77,0	77,2	**9,1%**	**14,7%**	**14,4%**
Code	64750	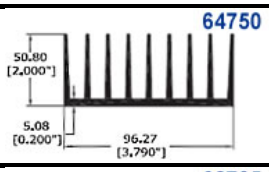	48,1	40	139	113,2	107,1	108,0	23,5%	29,1%	28,3%
Width (mm)	96,27		96,3	60	118	108,5	103,7	104,8	**11,0%**	16,5%	15,2%
Height (mm)	50,8		144	80	114	108,7	104,8	106,2	**5,8%**	**10,5%**	**8,8%**
fins	9		193	100	113	109,9	106,8	108,5	**3,4%**	**7,1%**	**5,0%**
Code	62705	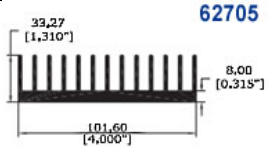	50,8	40	135	118,3	116,5	118,9	15,5%	17,2%	**14,9%**
Width (mm)	101,6		102	60	124	112,9	114,7	117,9	**12,2%**	**10,3%**	**6,9%**
Height (mm)	33,27		152	80	126	112,6	117,2	121,2	**14,1%**	**9,3%**	**5,2%**
fins	13		203	100	130	113,6	120,7	125,3	16,2%	**9,2%**	**4,5%**
Code	66430	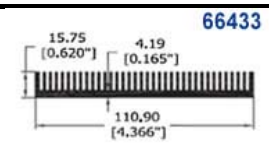	55,5	15	124	65,7	113,9	116,9	61,9%	**10,5%**	**7,3%**
Width (mm)	110,9		111	22,5	113	62,9	110,6	112,4	60,5%	**3,1%**	**1,0%**
Height (mm)	15,75		166	30	105	62,6	109,4	110,6	56,7%	**5,6%**	**7,2%**
fins	36		222	37,5	102	62,8	108,8	109,8	54,5%	**9,2%**	**10,5%**
Code	60560	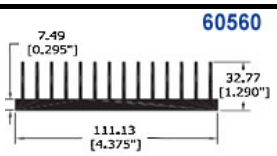	55,6	40	115	109,6	106,8	108,4	**6,2%**	**9,5%**	**7,6%**
Width (mm)	111,1		111	60	108	104,7	104,5	106,7	**4,7%**	**4,9%**	**2,2%**
Height (mm)	32,77		167	80	110	104,6	106,4	109,1	**6,3%**	**4,0%**	**0,6%**
fins	14		222	100	112	105,5	109,2	112,3	**7,7%**	**3,2%**	**0,7%**
Code	61075	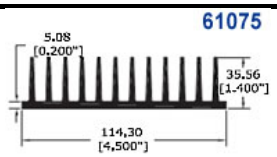	57,2	40	122	111,4	107,8	109,5	**11,2%**	15,0%	**13,2%**
Width (mm)	114,3		114	60	109	106,2	105,4	107,6	**3,5%**	**4,6%**	**1,8%**
Height (mm)	35,56		171	80	108	106,1	107,3	110,2	**2,5%**	**0,9%**	**2,8%**
fins	12		229	100	110	107,1	110,2	113,6	**3,5%**	**0,4%**	**4,6%**
Code	66142	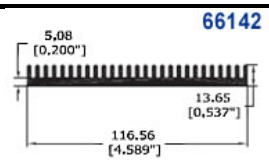	58,3	10	106	63,8	89,2	92,4	55,3%	21,6%	17,4%
Width (mm)	116,6		117	15	96,8	60,6	88,7	90,8	54,2%	**12,2%**	**9,0%**
Height (mm)	13,65		175	20	91,3	60,0	88,6	90,2	51,1%	**4,4%**	**1,9%**
fins	27		233	25	87,5	60,0	88,7	89,9	47,8%	**2,1%**	**4,2%**

Full Surface Heat Transfer		Aluminum Extrusion Profiles Ferraz Shawmut / Mersen	r-theta results			Junction temperature algorithm Results			% ERROR		
			Length (mm)	Heat (W)	T-junction (C)	Yovanovich (C)	Bil. Boundary (C)	Bil. Wall (C)	Yovanovich	Bil. boundary	Bil. wall
Code	66414	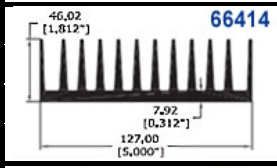	63,5	50	118	106,2	101,5	102,5	**13,0%**	18,4%	17,2%
Width (mm)	127		127	75	105	102,0	99,1	100,4	**4,4%**	**8,2%**	**6,5%**
Height (mm)	46,02		191	100	105	102,2	100,7	102,4	**3,9%**	**6,0%**	**3,7%**
fins	12		254	125	108	103,5	103,2	105,2	**5,1%**	**5,5%**	**2,9%**
Code	66344	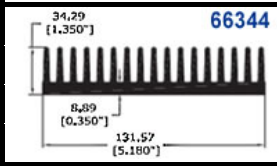	65,8	40	111	94,4	100,5	103,9	20,3%	**12,7%**	**8,5%**
Width (mm)	131,6		132	60	112	90,3	102,9	107,5	26,6%	**11,2%**	**5,6%**
Height (mm)	34,29		197	80	118	90,2	107,5	112,9	31,8%	**12,1%**	**6,0%**
fins	17		263	100	123	91,1	112,1	117,8	34,3%	**11,7%**	**5,6%**
Code	61790	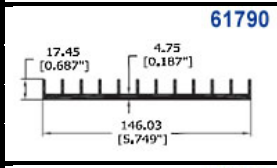	73	30	124	108,4	103,4	103,8	16,7%	22,0%	21,6%
Width (mm)	146		146	45	105	101,1	96,6	96,9	**5,0%**	**11,1%**	**10,6%**
Height (mm)	17,45		219	60	100	99,7	95,4	95,8	**1,0%**	**7,1%**	**6,6%**
fins	12		292	75	99,2	99,7	95,6	96,0	**0,7%**	**5,2%**	**4,6%**
Code	60230	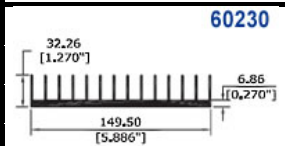	74,8	50	118	105,6	100,2	100,7	**13,9%**	20,2%	19,5%
Width (mm)	149,5		150	75	103	100,7	96,0	96,7	**3,7%**	**10,0%**	**9,1%**
Height (mm)	32,26		224	100	101	100,5	96,5	97,3	**1,0%**	**6,6%**	**5,5%**
fins	14		299	125	102	101,4	98,0	98,9	**0,6%**	**5,5%**	**4,2%**
Code	66451	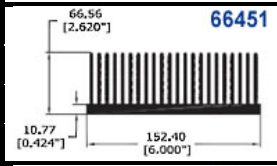	77,2	100	109	94,4	110,5	116,4	18,0%	**2,5%**	**10,0%**
Width (mm)	154,4		154	150	117	92,7	120,1	127,7	27,7%	**3,9%**	**12,6%**
Height (mm)	66,56		232	200	126	94,6	129,6	137,7	33,0%	**3,4%**	**11,7%**
fins	22		309	250	135	97,3	137,9	145,9	35,7%	**3,2%**	**10,8%**
Code	60140	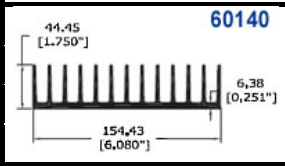	77,2	75	132	117,6	111,1	112,1	**14,0%**	20,4%	19,5%
Width (mm)	154,4		154	113	115	112,9	107,7	108,8	**2,7%**	**8,9%**	**7,5%**
Height (mm)	44,45		232	150	112	113,5	109,1	110,5	**1,5%**	**3,7%**	**2,1%**
fins	13		309	188	114	115,3	111,7	113,3	**2,0%**	**2,2%**	**0,3%**
Code	61070	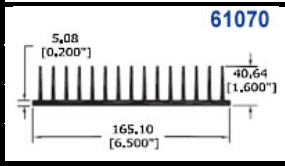	82,6	80	123	117,1	111,5	112,9	**6,7%**	**12,7%**	**11,3%**
Width (mm)	165,1		165	120	111	112,4	108,8	110,5	**2,3%**	**2,1%**	**0,0%**
Height (mm)	40,64		248	160	109	113,0	111,0	113,1	**4,6%**	**2,1%**	**4,7%**
fins	15		330	200	111	114,9	114,2	116,7	**4,3%**	**3,4%**	**6,5%**
Code	62285	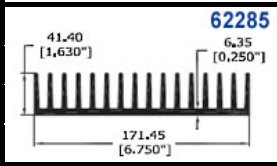	85,7	90	125	120,5	116,6	118,7	**4,8%**	**8,9%**	**6,6%**
Width (mm)	171,5		171	135	113	115,6	115,1	118,0	**2,9%**	**2,3%**	**5,8%**
Height (mm)	41,4		257	180	113	116,3	118,5	122,1	**4,3%**	**6,9%**	**11,3%**
fins	16		343	225	116	118,5	122,9	127,2	**3,3%**	**8,5%**	**13,5%**
Code	66449	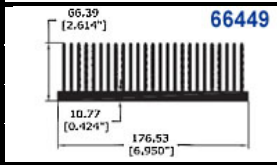	88,3	150	122	106,5	123,0	130,0	16,7%	**1,3%**	**8,9%**
Width (mm)	176,5		177	225	132	105,3	134,0	142,9	26,5%	**1,6%**	**10,3%**
Height (mm)	66,39		265	300	144	108,2	145,3	154,8	31,3%	**1,2%**	**9,6%**
fins	25		353	375	153	112,1	155,3	164,8	33,4%	**1,7%**	**9,3%**
Code	66279	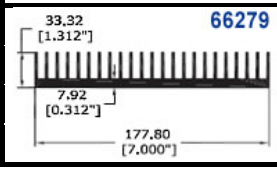	88,9	80	112	105,3	106,0	108,5	**7,9%**	**7,0%**	**3,9%**
Width (mm)	177,8		178	120	110	101,1	106,5	110,0	**11,4%**	**4,7%**	**0,3%**
Height (mm)	33,32		267	160	114	101,7	110,5	114,8	15,1%	**4,6%**	**0,5%**
fins	23		356	200	120	103,4	115,2	120,0	18,1%	**5,0%**	**0,4%**

Full Surface Heat Transfer		Aluminum Extrusion Profiles Ferraz Shawmut / Mersen	r-theta results			Junction temperature algorithm Results			% ERROR		
			Length (mm)	Heat (W)	T-junction (C)	Yovanovich (C)	Bil. Boundary (C)	Bil. Wall (C)	Yovanovich	Bil. boundary	Bil. wall
Code	66288	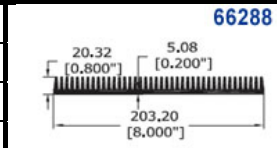	102	40	121	71,7	118,6	123,1	54,0%	**2,4%**	**2,5%**
Width (mm)	203,2		203	60	111	68,8	116,4	119,0	52,0%	**7,0%**	**10,2%**
Height (mm)	20,32		305	80	105	68,8	116,0	117,8	48,2%	**14,8%**	17,2%
fins	40		406	100	101	69,6	116,1	117,5	44,2%	21,3%	23,3%
Code	66226	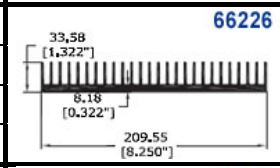	105	100	111	104,2	102,9	104,7	**8,5%**	**10,2%**	**7,9%**
Width (mm)	209,6		210	150	109	100,4	102,6	105,1	**10,3%**	**7,5%**	**4,3%**
Height (mm)	33,58		314	200	113	101,4	106,3	109,3	**14,0%**	**8,1%**	**4,4%**
fins	26		419	250	118	103,6	110,6	114,1	16,6%	**8,6%**	**4,6%**
Code	60815	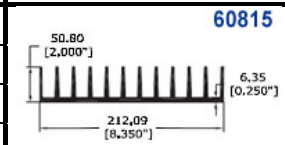	106	100	135	113,9	106,5	107,0	19,9%	26,9%	26,4%
Width (mm)	212,1		212	150	114	109,6	103,0	103,5	**5,2%**	**13,1%**	**12,6%**
Height (mm)	50,8		318	200	109	110,6	104,4	104,9	**1,6%**	**6,2%**	**5,6%**
fins	12		424	250	109	112,8	106,9	107,5	**5,4%**	**2,2%**	**1,5%**
Code	66179	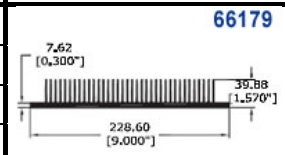	114	125	117	94,1	124,7	133,1	26,0%	**9,3%**	18,9%
Width (mm)	228,6		229	188	123	92,2	134,1	141,7	32,7%	**12,5%**	20,8%
Height (mm)	39,88		343	250	127	94,3	141,8	148,4	33,5%	15,6%	22,4%
fins	36		457	313	130	97,3	148,1	153,8	32,6%	18,4%	24,0%
Code	66180	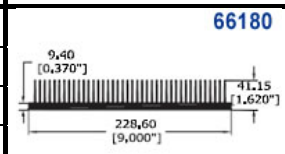	114	150	122	98,0	124,8	132,5	25,8%	**3,5%**	**11,9%**
Width (mm)	228,6		229	225	129	96,5	134,0	141,2	33,0%	**4,7%**	**11,9%**
Height (mm)	41,15		343	300	135	99,1	142,0	148,3	34,1%	**6,8%**	**12,7%**
fins	40		457	375	139	102,7	148,8	154,2	33,4%	**8,9%**	**13,8%**
Code	66434	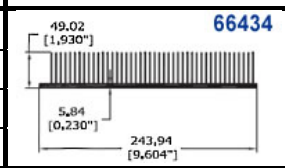	122	150	104	85,0	111,1	118,4	25,5%	**9,8%**	19,7%
Width (mm)	243,9		244	225	111	84,7	122,5	130,4	32,8%	**13,7%**	23,4%
Height (mm)	49,02		366	300	118	87,7	132,5	139,9	34,5%	16,4%	24,9%
fins	44		488	375	123	91,4	140,8	147,7	33,9%	19,2%	26,7%
Code	66221	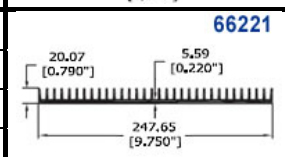	124	100	115	110,9	111,0	113,5	**5,0%**	**4,8%**	**1,8%**
Width (mm)	247,7		248	150	112	105,4	109,6	112,8	**8,5%**	**3,3%**	**0,5%**
Height (mm)	20,07		371	200	115	105,7	113,0	116,7	**10,9%**	**2,4%**	**2,0%**
fins	32		495	250	117	107,6	117,2	121,3	**10,8%**	**0,2%**	**4,9%**
Code	62725	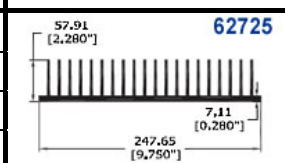	124	120	92,6	92,8	88,4	89,1	**0,3%**	**6,7%**	**5,5%**
Width (mm)	247,7		248	180	87,1	91,0	88,6	89,6	**6,9%**	**2,6%**	**4,4%**
Height (mm)	57,91		371	240	89,4	93,1	92,0	93,3	**6,2%**	**4,4%**	**6,6%**
fins	20		495	300	93,1	96,0	96,2	97,7	**4,6%**	**4,9%**	**7,3%**
Code	60520	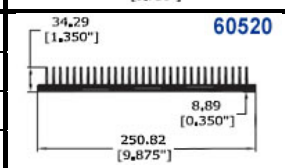	125	150	119	114,9	122,0	126,9	**5,0%**	**3,0%**	**8,5%**
Width (mm)	250,8		251	225	120	111,4	126,0	132,1	**9,9%**	**6,3%**	**13,1%**
Height (mm)	34,29		376	300	127	113,4	133,1	139,9	**13,7%**	**6,8%**	**13,8%**
fins	30		502	375	132	116,7	140,4	147,4	15,0%	**8,2%**	15,1%
Code	66428	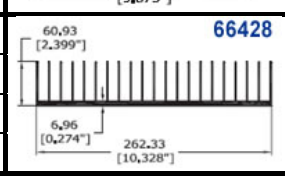	131	200	120	115,4	108,8	109,7	**5,0%**	**12,3%**	**11,3%**
Width (mm)	262,3		262	300	111	114,1	109,3	110,4	**4,2%**	**1,8%**	**0,4%**
Height (mm)	60,93		393	400	113	117,8	114,2	115,6	**5,3%**	**0,9%**	**2,6%**
fins	21		525	500	118	122,7	120,1	121,8	**5,1%**	**2,1%**	**4,1%**

Full Surface Heat Transfer		Aluminum Extrusion Profiles Ferraz Shawmut / Mersen	r-theta results			Junction temperature algorithm Results			% ERROR		
			Length (mm)	Heat (W)	T-junction (C)	Yovanovich (C)	Bil. Boundary (C)	Bil. Wall (C)	Yovanovich	Bil. boundary	Bil. wall
Code	66143	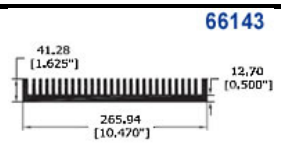	133	150	114	107,0	111,3	114,8	**8,2%**	**3,1%**	**1,0%**
Width (mm)	265,9		266	225	115	104,2	114,5	118,9	**12,3%**	**0,1%**	**5,1%**
Height (mm)	41,28		399	300	120	106,2	120,7	125,7	15,6%	**0,5%**	**6,0%**
fins	28		532	375	127	109,6	127,2	132,5	17,6%	**0,6%**	**6,1%**
Code	66395	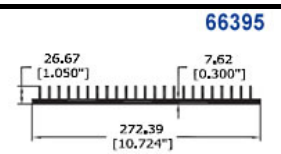	136	150	133	132,0	126,0	127,2	**0,7%**	**6,6%**	**5,4%**
Width (mm)	272,4		272	225	122	126,0	121,4	122,7	**4,8%**	**0,2%**	**1,2%**
Height (mm)	26,67		409	300	123	127,0	123,4	124,8	**4,9%**	**1,0%**	**2,5%**
fins	23		545	375	126	129,8	127,1	128,6	**4,2%**	**1,3%**	**3,0%**
Code	65340	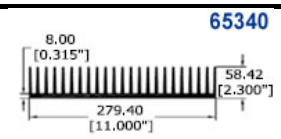	140	200	110	112,5	109,5	111,4	**3,7%**	**0,0%**	**2,4%**
Width (mm)	279,4		279	300	108	111,3	112,2	114,9	**3,7%**	**4,8%**	**8,2%**
Height (mm)	58,42		419	400	115	115,0	118,8	122,2	**0,2%**	**4,7%**	**8,7%**
fins	23		559	500	122	119,8	126,1	130,2	**2,5%**	**4,3%**	**8,7%**
Code	66427	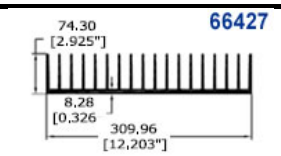	155	250	126	118,7	111,1	111,7	**7,6%**	15,6%	**14,9%**
Width (mm)	310		310	375	115	118,6	112,0	112,7	**4,5%**	**3,3%**	**2,5%**
Height (mm)	74,3		465	500	117	123,5	117,6	118,4	**8,1%**	**1,3%**	**2,2%**
fins	18		620	625	122	129,6	124,2	125,2	**8,7%**	**2,9%**	**3,9%**
Code	61155	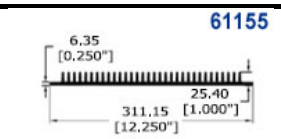	156	150	123	116,6	124,9	130,3	**6,5%**	**2,4%**	**8,2%**
Width (mm)	311,2		311	225	123	112,3	128,1	134,5	**11,8%**	**5,1%**	**12,0%**
Height (mm)	25,4		467	300	126	113,9	134,8	141,8	**12,3%**	**9,5%**	16,8%
fins	32		622	375	128	117,0	141,8	148,8	**11,0%**	**14,3%**	21,5%
Code	66459	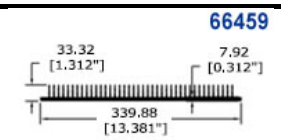	170	200	112	106,3	115,0	119,6	**6,7%**	**3,9%**	**9,5%**
Width (mm)	339,9		340	300	116	104,7	120,7	126,3	**12,6%**	**6,1%**	**12,7%**
Height (mm)	33,32		510	400	121	108,0	129,0	135,0	**14,4%**	**8,6%**	15,2%
fins	40		680	500	126	112,6	137,1	143,1	**13,9%**	**11,7%**	18,0%

If the error is below 15%, the error is highlighted with bold typography. Contrary, in errors exceeding 15% the number is colored red. In all profiles is considered a Rjc resistance of 0.05C/W

Appendix 2. AIR PROPIETIES AND EQUATIONS

Table of air proprieties

Temperature			Density	Volumetric thermal expansivity	Heat Capacity	Conductivity	Dynamic Viscosity	Kinematic viscosity	Prandtl
T			ρ	β	C_p	k	μ	ν	Pr
[C]	[F]	[K]	$\left[\frac{Kg}{m^3}\right]$	$\left[\frac{1}{K}\right]10^{-3}$	$\left[\frac{J}{Kg \cdot K}\right]$	$\left[\frac{W}{m \cdot K}\right]$	$\frac{[Pa \cdot s]}{10^6}$	$\frac{[m^2/s]}{10^6}$	
0	32	273	1,293	3,664	1003,9	0,02417	17,17	13,28	0,713
5	41	278	1,269	3,598	1004,3	0,02445	17,35	13,67	0,713
10	50	283	1,242	3,533	1004,6	0,02480	17,58	14,16	0,712
15	59	288	1,222	3,470	1004,9	0,02512	17,79	14,56	0,712
20	68	293	1,202	3,412	1005,2	0,02544	18,00	14,98	0,711
25	77	298	1,183	3,354	1005,4	0,02577	18,22	15,40	0,711
30	86	303	1,164	3,298	1005,7	0,02614	18,46	15,86	0,710
35	95	308	1,147	3,244	1006,0	0,02650	18,70	16,30	0,710
40	104	313	1,129	3,193	1006,3	0,02684	18,92	16,76	0,709
45	113	318	1,111	3,142	1006,6	0,02726	19,19	17,27	0,709
50	122	323	1,093	3,094	1006,9	0,02761	19,42	17,77	0,708
55	131	328	1,079	3,048	1007,3	0,02801	19,68	18,24	0,708
60	140	333	1,061	3,003	1007,7	0,02837	19,91	18,77	0,707
65	149	338	1,047	2,957	1008,0	0,02876	20,16	19,26	0,707
70	158	343	1,030	2,914	1008,4	0,02912	20,39	19,80	0,706
75	167	348	1,013	2,875	1008,8	0,02945	20,60	20,34	0,706
80	176	353	1,001	2,834	1009,3	0,02979	20,82	20,80	0,705
85	185	358	0,986	2,795	1009,8	0,03012	21,02	21,32	0,705
90	194	363	0,972	2,755	1010,3	0,03045	21,23	21,84	0,704
95	203	368	0,959	2,718	1010,7	0,03073	21,41	22,33	0,704
100	212	373	0,947	2,683	1011,2	0,03101	21,58	22,79	0,704

Proprieties equations

Fitted curves for air proprieties. Valid from 0 to 100 ºC.

Equations. Temperature *T* in Celsius degrees.	Units	R^2
$\rho = 9.8618 \cdot 10^{-6}T^2 - 4.3945 \cdot 10^{-3}T + 1.2884$	$\left[\frac{Kg}{m^3}\right]$	0,99966
$\beta = (3.1601 \cdot 10^{-5}T^2 - 1.2878 \cdot 10^{-2}T + 3.659)10^{-3}$	$\left[\frac{1}{K}\right]$	0,99992
$C_p = -4.3574 \cdot 10^{-11}T^6 + 1.3179 \cdot 10^{-8}T^5 - 1.5635 \cdot 10^{-6}T^4 + +9.4276 \cdot 10^{-5}T^3 - 2.8071 \cdot 10^{-3}T^2 + 9.2169 \cdot 10^{-2}T + 1003.9$	$\left[\frac{J}{Kg \cdot K}\right]$	0,99978
$k = -2.7725 \cdot 10^{-9}T^3 + 4.0404 \cdot 10^{-7}T^2 + 5.5634 \cdot 10^{-5}T + 2.4180 \cdot 10^{-2}$	$\left[\frac{W}{m \cdot K}\right]$	0.99995
$\mu = (-1.8732 \cdot 10^{-6}T^3 + 2.6013 \cdot 10^{-4}T^2 + 3.679 \cdot 10^{-2}T + 17.173)10^{-6}$	$[Pa \cdot s]$	0,99996
$\nu = (-3.4864 \cdot 10^{-8}T^4 + 5.4658 \cdot 10^{-6}T^3 - 9.6597 \cdot 10^{-5}T^2 + 8.4954 \cdot 10^{-2}T + 13.278)10^{-6}$	$[m^2/s]$	0,99996
$Pr = 4.63522 \cdot 10^{-9}T^3 - 6.09812 \cdot 10^{-7}T^2 - 7.86027 \cdot 10^{-5}T + 7.13087 \cdot 10^{-1}$		0,99992

R^2 is the square root of the correlation coefficient.

Appendix 3. Multiple heat source algorithm for Matlab.

Natural convection algorithm

```
function [Tj]=dissipateur
(Ld,wd,xd,yd,P,Rjc,Tamb,L,w,tp,Slibre,k,H,tab,taf,sb,na,Sem)

%Function. This function accepts Ld, wd,xd, yd, P, Rjc, Tamb, L, w, tp, Slibre, k, H, tab, taf, sb, na, Sem
variables and returns the junction temperature vector [Tj]. As sample, all previous are defined, taking as
model the 64750 profile. 3 Heat sources are also defined.

%Device parameters
%Ld=[0.04 0.04 0.04];                Device Length vector [m]
%wd=[0.025 0.025 0.025];             Device Width vector [m]
%xd=[0.05 0.05 0.05];                Device x position vector [m]
%yd=[0.075 0.15 0.225];              Device x position vector [m]
%P=[60 60 60];                       Device heat rate generation [W]
%Rjc=[0.05 0.05 0.05];               Resistance Junction-case [C/W]

%Heat Sink parameters

%Sem=0.77;                           Surface emmisivity
%L=0.3;                              Heat sink Length [m]
%w=0.09627;                          Heat sink width [m]
%tp=0.00508;                         Plate thickness [m]
%Slibre=0                            Part od the plate width without fins [m]
%k=210;                              Conductivity of the material of the Heat Sink [W/mK]
%H=0.046;                            Fin height [m]
%tab=3.466E-3;                       Fin base thickness [m]
%taf=2.124E-3;                       Fin tip thickness [m]
%sb=8.135E-3;                        Interfin space at base [m]
%na=9;                               Number of fins

%Ambient Parameter

%Tamb=30;                            Ambient temperature [C]

Ab=w*L;                              %Sink total surface [m^2]

%Air proprieties

Tm=@(Ts) (Ts+Tamb)/2;                %Film temperature[C]
Betaa=@(T) 1/(T+273);                % Volumetric thermal expansivity [1/K]
Prandtl=@(T) 4.63522E-9*T^3-6.09812E-7*T^2-7.86027E-5*T+7.13087E-1; %Prandtl
number function
Kinvis=@(T) (-3.4864E-8*T^4+5.4658E-6*T^3-9.6597E-5*T^2+8.4954E-
2*T+1.3278E1)*1E-6;   %Kinematic viscosity [m^2/s]
Dynvis=@ (T) (-1.8732E-6*T^3+2.6013E-4*T^2+3.679E-2*T+17.173)*1E-6; % Dynamic
viscosity [Pa·s]
ka=@(T) -2.7725E-9*T^3+4.0404E-7*T^2+5.5634E-5*T+2.418E-2; %Air thermal
conductivity [W/mK] alpha=@(T)Kinvis(T)/Prandtl(T); %Thermal diffusivity [m^2/s]
Dens=@ (T) 9.8618E-6*T^2-4.3945E-3*T+1.2884; %Thermal density [Kg/m^3]
Cp=@ (T) -4.3574E-11*T^6+1.3179E-8*T^5-1.5635E-6*T^4+9.4276E-5*T^3-2.8071E-
3*T^2+9.2169E-2*T+1.0039E3; %Air Heat Capacity [Kg/m^3]
```

```
%Total power generated [W]

Nd=length(Ld);
Ptot=0;
for b=1:Nd
    Ptot=P(b)+Ptot;

end

Hc=H+taf/2;                    %Fin height correction [m]
Ap=(Slibre+(na-1)*sb)*L;       %Primary surface [m^2]
Af=Hc*2*na*L;                  %Fin surface [m2]
kappa=atan((tab-taf)/(2*H));   %Fin angle [rad]
sm=(2*sb+tab-taf)/2;           %Average Interfin space [m]
g=9.81;                        %Gravity [m/s^2]
sigma=5.6704E-8;               %Stefan-Boltzmann constant

%Fin efficiency for a trapezoidal profile

K=@(h) sqrt(h/(k*sin(kappa)));
mua=@(h) 2*K(h)*sqrt(taf*(1-tan(kappa))/(2*tan(kappa)));
mub=@(h) 2*K(h)*sqrt(H+taf*(1-tan(kappa))/(2*tan(kappa)));
eff=@(h) (mub(h)/(2*H*(K(h))^2))*(besselk(1,mua(h))*besseli(1,mub(h))-
besseli(1,mua(h))*besselk(1,mub(h)))/(besseli(0,mub(h))*besselk(1,mua(h))+b
esseli(1,mua(h))*besselk(0,mub(h)));

%CONVECTION COEFFICIENT. CHOICE ONE OF THIS THREE PROPOSED CONVECTION MODELS.

%CONVECTION COEFFICIENT BY YOVANOVICH

S=(na*(2*(((tab+taf)/2)^2+H^2)^0.5+taf)+(w-na*tab))*L;
RaS=@(Ts) (g*Betaa(Tm(Ts))*Prandtl(Tm(Ts))*(Ts-
Tamb)*S^1.5)/(Kinvis(Tm(Ts))^2);                    %RaS Rayleich number

f=@ (Ts) 0.67/(1+(0.5/Prandtl(Tm(Ts)))^(9/16))^(4/9);   %Universal Prandtl
function
Nudl=(3.192+1.868*(H/L)^0.76)/(1+1.189*(H/L))^0.5;      %Diffusive limit
Lambda=na*H+tp+w;
GS=2^(1/8)*((L*(H*na+tp+w)^2)/((tab/2+taf/2)*H*na+tp*w+L*(H*na+tp+w))^1.5)^
0.25;                                                   %Body
function
NuS=@(Ts) Nudl+f(Ts)*GS*(RaS(Ts))^0.25;                 %Nusselt number
hc=@ (Ts) ka(Tm(Ts))*NuS(Tm(Ts))/(S^0.5);               %Convection
coefficient

%CONVECTION COEFFICIENT BY BILITZKY AT Ts

r=2*H*sm/(2*H+sm);
a=sm/H;
B=1.25*(1+sm/(2*H));
Lambda1=1-0.483*exp(-0.17/a);
Lambda2=1-exp(-0.83*a);
Lambda3=9.14*(a.^0.5)*exp(-B)-0.61;
Psi=24*Lambda1/(((1+a/2)*(1+Lambda2*Lambda3)).^3);
Rar=@(Ts) ((Dens(Ts)^2)*g*Betaa(Tm(Ts))*Cp(Ts)*(Ts-
Tamb)*r^3)/(Dynvis(Ts)*ka(Ts));                     %RaS Rayleich number

El=@(Ts) Rar(Ts)*r/L;                               % Elenbaas number
```

```
Nur=@(Ts) El(Ts)*(1-exp(-Psi*((0.5/El(Ts)).^0.75)))/Psi;    %Nusselt number
hc= @(Ts) Nur(Ts)*ka(Ts)/r;                                 %Convection
coefficient
```

```
%CONVECTION COEFFICIENT BY BILITZKY AT Tm

r=2*H*sm/(2*H+sm);
a=sm/H;
B=1.25*(1+sm/(2*H));
Lambda1=1-0.483*exp(-0.17/a);
Lambda2=1-exp(-0.83*a);
Lambda3=9.14*(a.^0.5)*exp(-B)-0.61;
Psi=24*Lambda1/(((1+a/2)*(1+Lambda2*Lambda3)).^3);
Rar=@(Ts) ((Dens(Tm(Ts)^2)*g*Betaa(Tm(Ts))*Cp(Tm(Ts)*(Ts-
Tamb)*r^3)/(Dynvis(Tm(Ts)*ka(Tm(Ts));                       %RaS Rayleich number
El=@(Ts) Rar(Ts)*r/L;                                       %Elenbaas number
Nur=@(Ts) El(Ts)*(1-exp(-Psi*((0.5/El(Ts)).^0.75)))/Psi;    %Nusselt number
hc= @(Ts) Nur(Ts)*ka(Ts)/r;                                 %Convection
coefficient
```

```
%RADIATION CALCULATION

Hr=H/sm;
Lr=L/sm;
Fs=1-2*Hr*((1+Lr.^2).^0.5-1)/(2*Hr*Lr+(1+Lr.^2).^0.5-1);
Qch=@(Ts) sigma*(sm+2*H)*L*((Ts+273.15).^4-(Tamb+273.15).^4)/(((1-
Sem)/Sem)+1/Fs);
Qtr=@(Ts)
na*Qch(Ts)+(na*tp*(L+2*H)+2*H*L+2*tp*(L+w))*sigma*Sem*((Ts+273).^4-
(Tamb+273.15).^4);
Ahs=Ap+Af+tp*2*(w+L)+na*(tab+taf)*(2*H+L)/2;
hr=@(Ts) Qtr(Ts)/(Ahs*(Ts-Tamb));
```

```
%SPREADING CALCULATION

Phi=@(zeta,h)
((zeta*sinh(zeta*tp))+(h*cos(zeta*tp)/k))/((zeta*cosh(zeta*tp))+(h*sinh(zet
a*tp)/k));
```

```
%ITERATION PROCESS

%Ts evaluation

Pnouvell=0.1;
j=1;
Error=100;
Ts=Tamb+90;
iter=1;
while Error>0.001
    h=hr(Ts)+hc(Ts);
    Ts1=(Ptot/(h*(Ap+eff(h)*Af)))+Tamb;
    Error=abs(Ts1-Ts);
    Ts=Ts1;
    iter=iter+1;
end
```

```
%Evaluation of  the Temperature drop vector
```

```
%ITERATION PROCESS

hm=(Ap+eff(h)*Af)*h/Ab;
for j=1:Nd
    theta1(j)=0;
    for i=1:Nd
        A0(i)= P(i)*((tp/k)+(1/hm))/(w*L);
        sum1=0;
        sum2=0;
        sum3=0;
        for m=1:100
            lambda=(m*pi)/w;
           Am=2*P(i)*(sin(((2*xd(i)+wd(i))*lambda/2))-sin((2*xd(i)-
           wd(i))*(lambda/2)))/(w*L*wd(i)*k*(lambda.^2)*Phi(lambda,hm));

      sum1=(Am*cos(lambda*xd(j))*sin(lambda*wd(j)/2)/(lambda*wd(j)))+sum1;
        end
        for n=1:100
            delta=(n*pi)/L;
           An=2*P(i)*(sin((2*yd(i)+Ld(i))*delta/2)-sin((2*yd(i)-
           Ld(i))*delta/2))/(w*L*Ld(i)*k*(delta.^2)*Phi(delta,hm));
           sum2=(An*cos(delta*yd(j))*sin(delta*Ld(j)/2))/(delta*Ld(j))+sum
           2;
        end
        for m=1:100
            for n=1:100
                  lambda=(m*pi)/w;
                  delta=(n*pi)/L;
                  beta=sqrt((lambda.^2)+(delta.^2));
                  Amn=(16*P(i)*cos(lambda*xd(i))*sin(lambda*wd(i)/2)*cos(de
                  lta*yd(i))*sin(delta*Ld(i)/2))/(w*L*wd(i)*Ld(i)*k*beta*la
                  mbda*delta*Phi(beta,hm));
                  sum3=(Amn*cos(delta*yd(j))*sin(delta*Ld(j)/2)*cos(lambda*
                  xd(j))*sin(lambda*wd(j)/2))/(lambda*wd(j)*delta*Ld(j))+su
                  m3;
            end
        end
        theta(i,j)=A0(i)+2*sum1+2*sum2+4*sum3;
    end
    for i=1:Nd
        theta1(j)=theta(i,j)+theta1(j);
    end
end

%Junction temperature vector evaluation

for j=1:Nd
    Tc(j)=theta1(j)+Tamb;
    Tj(j)=Tc(j)+P(j)*Rjc(j);
end
```